The endocannabinoid system dual-target ligand *N*-cycloheptyl-1,2-dihydro-5-bromo-1-(4-fluorobenzyl)-6-methyl-2-oxo-pyridine-3-carboxamide improves disease severity in a mouse model of multiple sclerosis

Chiara Arena,[⊥,Ψ] Francesca Gado,[⊥] Lorenzo Di Cesare Mannelli,[§] Chiara Cervetto,[δ] Sara Carpi,[⊥] Ines Reynoso-Moreno,[Ψ] Beatrice Polini,[⊥] Erika Vallini,[⊥,Ψ] Stefano Chicca,[⊥,Ψ] Elena Lucarini,[§] Simone Bertini,[⊥] Felicia D'Andrea,[⊥] Maria Digiacomo,[⊥] Giulio Poli,[⊥] Tiziano Tuccinardi,[⊥] Marco Macchia,[⊥] Jürg Gertsch,[Ψ] Manuela Marcoli,[δ] Paola Nieri,[⊥] Carla Ghelardini,[§] Andrea Chicca,[Ψ,*] Clementina Manera[⊥,*]

[⊥]Department of Pharmacy, University of Pisa, 56126 Pisa, Italy. [Ψ]NCCR-TransCure, Institute of Biochemistry and Molecular Medicine, University of Bern, CH-3012 Bern, Switzerland. [§]Department of Neuroscience, Psychology, Drug Research and Child Health, Section of Pharmacology and Toxicology, University of Florence, 50139 Florence, Italy.[δ] Department of Pharmacy, Section of Pharmacology and Toxicology, University of Genova, 16126 Genova, Italy.

Corresponding Authors
*Clementina Manera: Phone: +39 050 2219548. Fax: +39 050 2210680. e-mail: clementina.manera@farm.unipi.it.
*Andrea Chicca: e-mail: andrea.chicca@ibmm.unibe.ch

ORCID
Clementina Manera: 0000-0002-7379-5743

Felicia D'Andrea: 0000-0003-1517-4911

Maria Digiacomo: 0000-0003-0653-6642

Tiziano Tuccinardi: 0000-0002-6205-4069

Andrea Chicca: 0000-0001-9593-636

Notes

The authors declare no competing financial interest.

RECEIVED DATE (to be automatically inserted after your manuscript is accepted if required according to the journal that you are submitting your paper to)

Highlights

- We synthesized 1,2-dihydropyridine-2-oxo-3-carboxamides with dual-activity on ECS
- The derivative **B2** reduced LPS-induced activation of microglial cells
- The derivative **B2** reduced glutamate release from rat synaptosomes
- The derivative **B2** showed activity on EAE model of multiple sclerosis
- The derivative **B2** demonstrated antinociceptive effects on neuropathic pain model

Graphical abstract

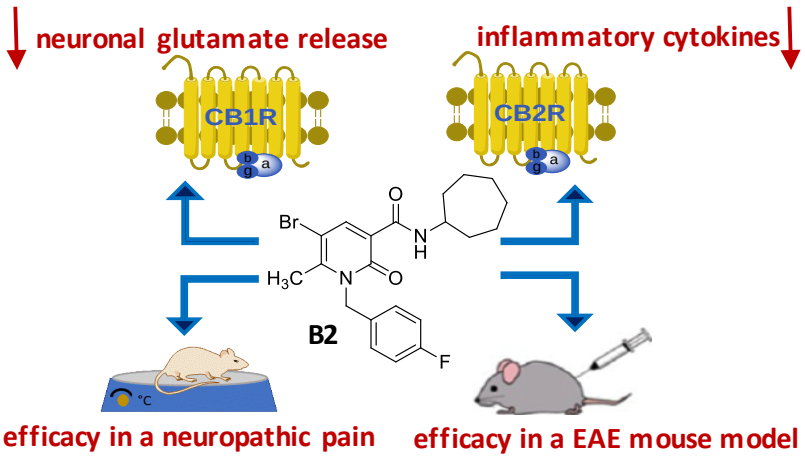

ABSTRACT

Multiple sclerosis is a chronic inflammatory demyelinating disorder of the central nervous system that eventually leads to progressive neurodegeneration and disability. Recent findings highlighted the emerging role of each target of the endocannabinoid system in controlling the symptoms and disease progression of multiple sclerosis. Therefore, multi-target modulators of the endocannabinoid system could provide a more effective pharmacological strategy as compared to the single target modulation. In this work, N-cycloheptyl-1,2-dihydro-5-bromo-1-(4-fluorobenzyl)-6-methyl-2-oxo-pyridine-3-carboxamide (**B2**) was identified as the most promising compound with dual agonism at cannabinoid receptors type-1 and cannabinoid receptors type-2 and good drug-like properties. In *in vitro* assays, **B2** reduced glutamate release from rat synaptosomes through interaction with cannabinoid receptors type-1 and modulated the production of the pro- and anti-inflammatory cytokines (interleukins IL-1β and IL-6 and interleukin IL-10 respectively) via cannabinoid receptors type-2 activation. Furthermore, **B2** demonstrated antinociceptive effects in an animal model of neuropathic pain and efficacy in an experimental autoimmune encephalomyelitis model of multiple sclerosis.

Keywords: endocannabinoid system, 1,2-dihydropyridine-2-oxo-3-carboxamides, microglial cell, glutamate release, neuropathic pain, EAE mouse model multiple sclerosis.

1. Introduction

Over the past years, a great amount of preclinical studies highlighted that compounds targeting the endocannabinoid system (ECS) exert anti-inflammatory, neuroprotective and immuno-modulatory effects [1-11], allowing to alleviate symptoms and limit progressive neurodegeneration in animal models of multiple sclerosis (MS) [12]. The ECS is a complex lipid signaling system mainly composed of at least two G-protein coupled receptors, cannabinoid receptors type-1 (CB1R) and type-2 (CB2R), and endogenous bioactive lipids known as endocannabinoids (ECs), from which the most abundant and well-studied are anandamide (AEA) and 2-arachidonoylglycerol (2-AG). The biological activities of these lipid mediators are terminated upon cellular re-uptake and subsequent metabolism. The main metabolic enzymes of ECs are fatty acid amide hydrolase (FAAH) that degrades AEA to arachidonic acid (AA) and ethanolamine, and monoacylglycerol lipase (MAGL) that degrades 2-AG to AA and glycerol [13]. The first evidence to support the involvement of the ECS in MS was obtained in the early 1990s' from MS patients that frequently reported self-medication with cannabis to alleviate MS symptoms, in particular pain and muscle spasticity. The latter seems to be mostly mediated by CB1R activation [14]. Besides direct receptor agonism (i.e. Δ9-THC), CB1R activation can be achieved by elevation of endogenous ligands (i.e. ECs) through inhibition of endocannabinoid cell reuptake [15], or enzymatic degradation [16,17].

Endocannabinoids exert neuroprotective effects acting at multiple molecular sites, that are in all key cellular elements for the control of neuronal survival (e.g., neurons, astrocytes, resting and reactive microglia, oligodendrocytes) and also in key brain structures (e.g., blood–brain barrier, BBB) [18]. Cannabinoids can limit excitotoxicity by acting on CB1R in neurons, reduce toxic influence of reactive microgliosis by activation of CB2R in microglial cells, and enhance the

trophic and metabolic support to neurons by activating CB1R or CB2R in astroglial cells. In particular, CB1R-mediated neuroprotection is associated to the reduction of glutamate release which is a key mediator of neuronal and oligodendrocyte damage in MS [19]. Indeed, oligodendrocyte excitotoxicity is ameliorated by MAGL inhibitors *via* enhancing endogenous levels of 2-AG [20].

Additionally, several studies suggest that the ECS provides a therapeutic target for treating microglial-derived neuroinflammation and that the ECS may regulate different aspects of neuroinflammation, including the balance between pro- and anti-inflammatory cytokines released by these cells [21]. Microglial cells have a functional endocannabinoid signaling system and express CB1R, CB2R and the complete machinery of EC biosynthetic and degrading enzymes. The protective role of CB2R activation in microglial cells during neuroinflammation was demonstrated in preclinical models of MS [22]. The AEA uptake inhibitor OMDM-2 exerted anti-inflammatory and neuroprotective effects in the Theiler encephalomyelitis virus-induced demyelinating mouse model of MS by counteracting neuroinflammation and reducing microglial reactivity [23].

On the basis of what reported above, it is evident that modulation of the ECS may offer a promising novel therapeutic strategy to control of symptoms and disease progression in MS. Multi-target modulators of the ECS can directly and indirectly modulate CB1R, CB2R and other ECS targets via different mechanisms of action [6, 24-31]. These molecules can potentially provide an improved therapeutic profile in terms of efficacy and side effects as compared to single target modulators.

Previously, our group reported the synthesis and biological evaluation of a series of compounds with general structure A (Figure 1) which exhibited interesting multi-target profiles within the

ECS [24]. In this work we developed a new class of compounds, **B** (Figure 1, Table 1), in which the aryl group at position 6 of **A** was substituted by a methyl group. The modification of the general structure **A** was based on the observation that the phenyl ring at position 6 of the best compound of the series **A** (compound **B1** in ref. 24) was predicted to be placed into a pocket of CB2R occupied by the phenyl ring of the antagonist AM10257, co-crystallized with CB2R (PDB code 5ZTY). This was consistent with the inverse agonist activity on CB2R observed for **B1** [24]. However, agonist compounds co-crystallized with CB1R with binding modes similar to AM10257 and **B1** showed to leave the corresponding pocket unoccupied. Based on these considerations, we envisioned that replacing the phenyl ring at position 6 with a smaller substituent such as a methyl group could let us obtain novel derivatives endowed with CB1R and CB2R agonist activity.

The new compounds are characterized by the presence of a *p*-fluorobenzyl moiety at the N-1 position of the 1,2-dihydro-2-oxo-pyridine ring, a *N*-cycloheptyl carboxamide group at the 3-position and different substituents at position 5 (R) that were chosen on the basis of the best results obtained with the previous series [24,25,32,33]. Furthermore, the cycloheptyl ring of the carboxamide group (R2) was also substituted with a *N*-piperidinyl moiety or polyhydroxylated structures as carbohydrates. Carbohydrates are involved in several biological processes and are therefore an intense subject of investigation for the development of future generation of drugs [34-36]. Furthermore, due to their polyhydroxylated nature, carbohydrates have also been employed just as safe, biocompatible enhancers of the hydrophilic character of otherwise water insoluble molecules [37].

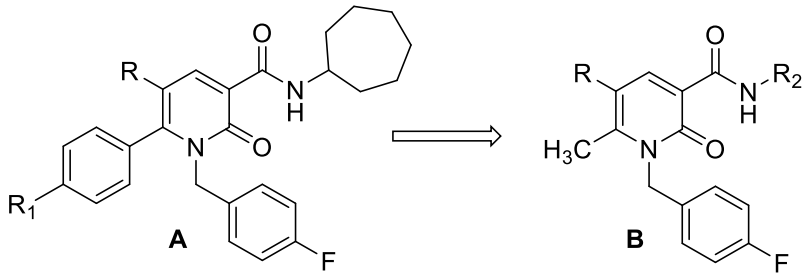

Figure 1. General structure of compounds **A** and **B**.

Compounds **B** were evaluated for their binding affinities (K_i values) for both CB1R and CB2R. Subsequently, the compounds with highest binding affinity to CBRs were investigated for their functional activity with [^{35}S]GTPγS assays to identify the behaviour as agonist, antagonist or inverse agonist for CBRs-induced G-protein-dependent signaling. All the synthesized compounds were also tested on the other main targets of the ECS (MAGL, FAAH, ABHD6 and ABHD12). From all these activities, we identified derivative **B2** (Table 1) as the most promising compound based on potent activation of both CB1R and CB2R, moderate inhibition of FAAH activity, and good drug-like properties. In functional assays, **B2** reduced depolarization-evoked glutamate release from rat synaptosomes by activation of CB1R and modulated pro- and anti-inflammatory cytokines production in activated mouse microglial cells by activation of CB2R. Finally, **B2** demonstrated its efficacy *in vivo* by improving disease severity in the EAE mouse model of MS and reducing pain in an acute model of oxaliplatin-induced neuropathic pain.

2. RESULTS AND DISCUSSION

2.1. Chemistry.

The synthesis of 1,2-dihydro-6-methyl-2-oxo-pyridine-3-carboxamides derivatives of general structure **B** was achieved through the synthetic pathway depicted in Schemes 1 and 2.

As described in Scheme 1, compound **B1** was prepared starting from the commercially available 2-hydroxy-6-methyl-nicotinic acid that was treated with the coupling agent 2-[(1H-benzotriazole-1-yl)-1,1,3,3-tetramethyluronium tetrafluoroborate] (TBTU) in the presence of triethylamine at 0 °C for 30 minutes. After that, cycloheptylamine was added and the reaction mixture was stirring at 0 °C for 30 minutes and then at room temperature for 12 h to give the desired carboxamide derivative **1**. Compound **1** was firstly treated with cesium carbonate in anhydrous DMF at room temperature for 1 h, and then with *p*-fluorobenzyl chloride, affording the desired *N*-alkylated derivative **B1** together to the corresponding *O*-substituted derivative **C1** in according to previously reported [24,25,32,33]. The two structural isomers were purified by flash chromatography.

As reported in Scheme 1, the treatment of carboxamide **1** with a solution of bromine in chloroform, afforded the corresponding derivative **2** which was *N*- alkylated using the same two-steps procedure described above, to give compound **B2**. The purification of **B2** by flash chromatography enabled us to obtain the corresponding *O*-alkylated compound **C2** in according to previously reported [24,25,32,33].

The synthesis of the halogen derivatives **B3** and **B4** was achieved starting from the carboxamide **1** which was treated with *N*-chlorosuccinimide using acetonitrile as solvent, at room temperature, for 12 h to afford the corresponding 5-chloro derivative **3**. In order to obtain the 5-fluoro derivative **4**, compound **1** was treated with 1-chloromethyl-4-fluoro-1,4-diazoniabicyclo[2.2.2]octane bis(tetrafluoroborate) at reflux acetonitrile for 12 h. The 5-halogenated-3-carboxamides **3** and **4** were then alkylated using the same two-step procedure already described, to give the *N*-alkylated compounds **B3** and **B4**.

Scheme 1. Synthesis of the 1,2-dihydro-6-methyl-2-oxo-pyridines **B1-B10** and 2-substituted pyridines **C1, C2, C6** and **C7**

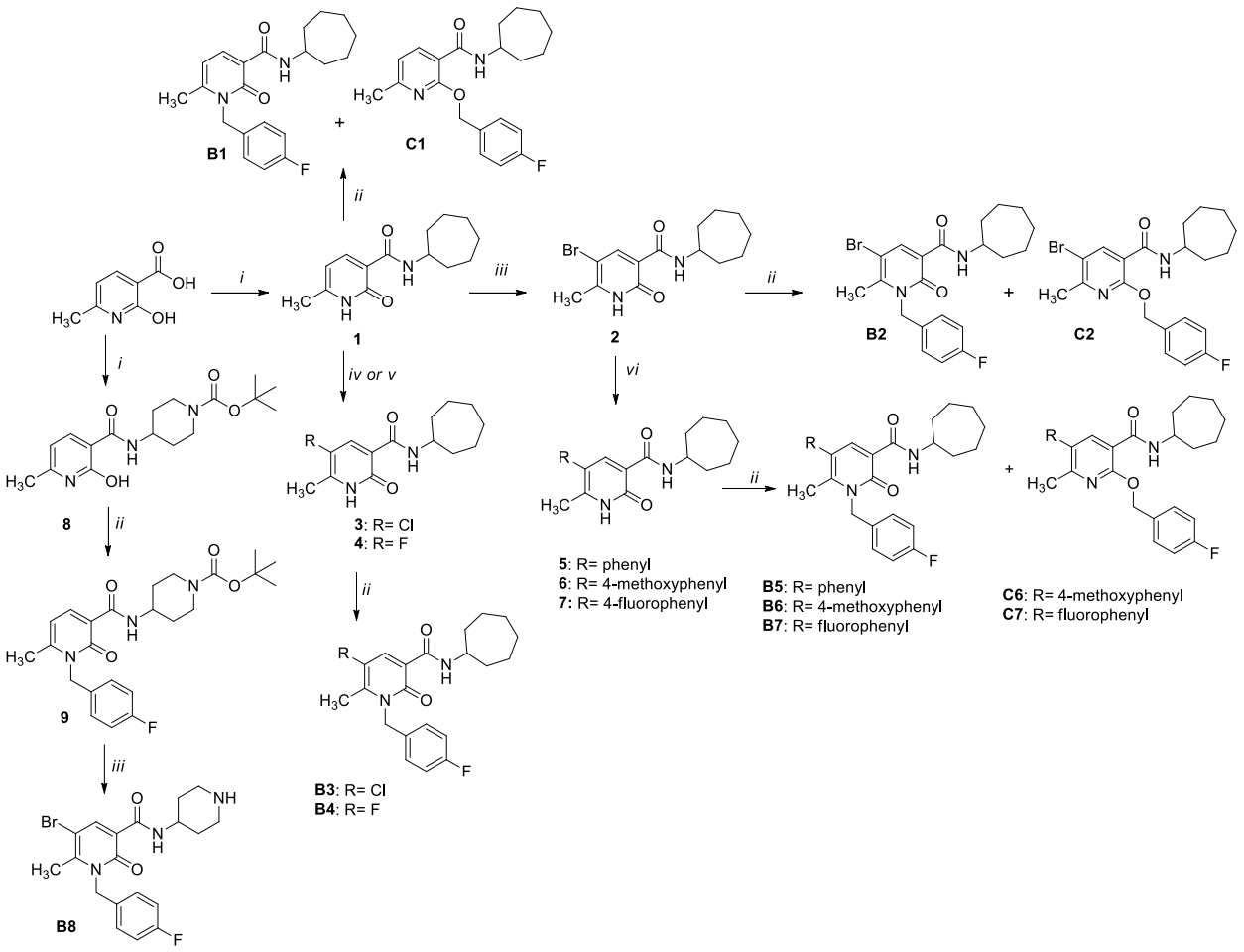

Reagents and conditions: (i) 1) suitable amine, TBTU, Et_3N, DMF, 0 °C; 2) rt, 12 h; (ii) 1) Cs_2CO_3, anhydrous DMF, rt, 1 h; 2) *p*-fluorobenzyl chloride, 25 °C, 12 h; (iii) Br_2, $CHCl_3$, rt, 12 h; (iv) *N*-chlorosuccinimide, CH_3CN, rt, 12 h; (v) 1-chloromethyl-4-fluoro-1,4-diazoniabicyclo[2.2.2]octane bis(tetrafluoroborate), CH_3CN, reflux, 12 h; (vi) suitable arylboronic acid, $Pd(OAc)_2$, PPh_3, 1,4-dioxane, 2 M Na_2CO_3 aqueous, MW 110 °C, 1 h (power: 200 W, pressure: 100 psi, under stirring).

The synthesis of compounds **B5-B7** (Scheme 1) was accomplished from the 5-bromo derivative **2** which was subjected to a Suzuki-Miyaura cross-coupling reaction with the suitable boronic acid (phenyl, *p*-methoxyphenyl or *p*-fluorophenyl boronic acid) in the presence of tetrakis(trisphenylphosphine)palladium(0) (prepared *in situ* using triphenylphosphine and palladium acetate) as the catalyst and 2 M sodium carbonate aqueous solution as the base and carried out under microwave irradiations. The obtained 5-substituted derivatives **5**, **6** and **7** reacted with *p*-fluorobenzyl chloride, affording compounds **B5**, **B6** and **B7**, that were purified by flash chromatography. The purification of **B6** and **B7** also enabled us to obtain the corresponding *O*-alkylated compound, **C6** and **C7** respectively were also isolated in according to previously reported [24,25,32,33].

Compound **B8** (Scheme 1) was obtained from 2-hydroxy-6-methyl-nicotinic acid which was treated with the coupling agent TBTU as described above and then with 4-amino-piperidine-1-carboxylic acid *t*-butyl ester to give the amino derivative **8**. Compound **8** was then *N*-alkylated as already reported, to give compound **9** which was treated with a solution of bromine in chloroform to afford the final compound **B8**.

The glycoconjugates **B9** and **B10** were prepared as described in Scheme 2. The 2-hydroxy-6-methyl-nicotinic acid was *N*-alkylated by treatment with *p*-fluorobenzyl chloride in the presence of CsF in anhydrous DMF to afford the carboxylic acid **10**. This compound was treated with the coupling agent TBTU as described above and then with monosaccharide derivatives **11** [38] or **12** [39] to obtain the glycoconjugates **13** and **14** respectively. The treatment of **13** with a solution of bromine in chloroform directly afforded the desired compound **B9**. In the case of compound **14**, the same reaction gave the glycoconjugate **15** which by alkaline hydrolysis provided the desired compound **B10**.

Scheme 2. Synthesis of glycoconjugates **B9** and **B10**.

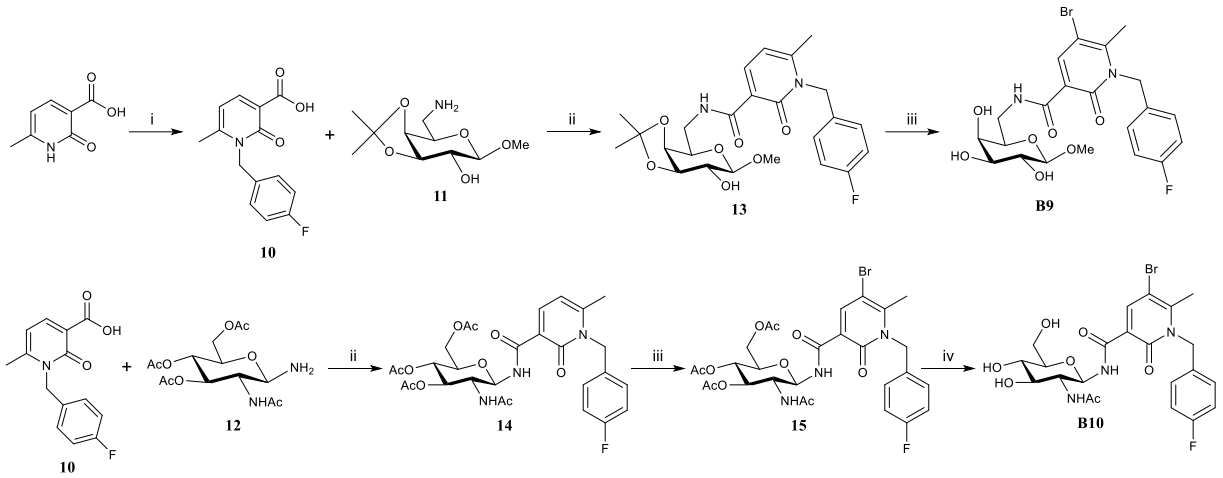

Reagents and conditions: (i) 1) CsF, anhydrous DMF, rt, 1 h; 2) *p*-fluorobenzyl chloride, 50 °C, 12 h; 3) NaOH 10%, reflux, 12 h; 4) HCl 1 N; (ii) suitable amine, TBTU, Et_3N, DMF, 0 °C, rt, 12 h; (iii) Br_2, $CHCl_3$, rt, 12 h; (iv) NH_3-MeOH 3.5 N, rt, 24 h.

2.2. Polypharmacology in the ECS and Structure-Activity Relationships.

1,2-dihydro-2-oxopyridine derivatives **B1-B10** and 2-substituted pyridines **C1, C2, C6 *and* C7** were tested on the main targets of the ECS (CBRs, MAGL, FAAH and ABHDs). The results are reported in Table 1 and Table 2. The binding affinities (Table 1, K_i values) of novel compounds were evaluated in competitive radioligand displacement assays against [^{3}H]CP-55,940 using membrane preparations obtained in-house from stable transfected CHO-*h*CB1 and CHO-*h*CB2 cells. (R)-WIN55,212 was used as positive control for both CB1R and CB2R binding experiments and showed K_i value of 2.5 ± 0.9 nM for CB1R and 1.6 ± 0.5 nM for CB2R.

Table 1. Data of 1,2-dihydro-2-oxopyridine **B1-B10** and pyridine-3-carboxamide derivatives **C1, C2, C6** and **C7**.[a]

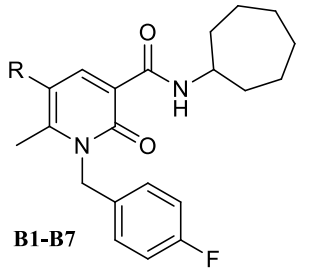

B1-B7

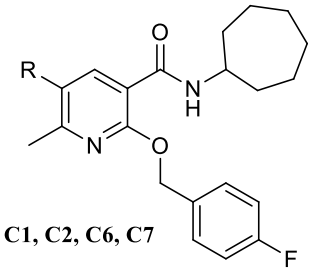

C1, C2, C6, C7

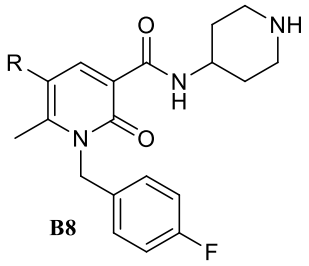

B8

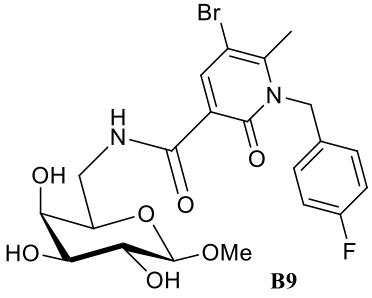

B9

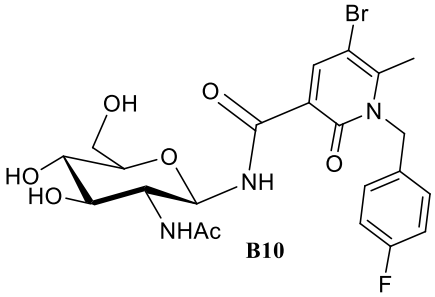

B10

		K_i value (mean ± SD, nM)		IC$_{50}$ (mean ± SD, μM)			
Cmpds	**R**	**CB1R**	**CB2R**	**FAAH**	**MAGL**	**ABHD6**	**ABHD12**
B1	H	37.7 ± 79.1	4.7 ± 2.6	>10	>10	>10	>10
B2	Br	2.9 ± 1.2	1.5 ± 0.8	5.9 ± 0.5	>10	>10	>10
B3	Cl	3.7 ± 8.4	4.3 ± 2.3	5.9 ± 0.4	>10	>10	>10
B4	F	4.9 ± 3.7	5.7 ± 2.6	>10	>10	>10	>10
B5	Phenyl	176 ± 187	5.7 ± 7.5	0.56 ± 0.11	>10	>10	>10
B6	*p*-OCH$_3$phenyl	9.8 ± 8.5	26.2 ± 18.3	2.0 ± 0.2	>10	0.53 ± 0.22	>10
B7	*p*–Fluorophenyl	49.3 ± 15.1	28.9 ± 6.7	0.53 ± 0.09	>10	>10	0.6 ±1.2
B8	Br	>10000	>10000	>10	>10	>10	>10
B9	Br	>10000	>10000	>10	>10	>10	>10

B10	Br	>10000	>10000	>10	>10	>10	>10
C1	H	16.6 ± 16.2	33.9 ± 21.6	>10	>10	>10	>10
C2	Br	76.1 ± 78.9	1.5 ± 1.9	>10	>10	>10	2.1 ± 0.7
C6	*p*-OCH_3phenyl	>10000	919 ± 502	>10	>10	0.53 ± 0.24	>10
C7	*p*–Fluorophenyl	4600 ± 1201	531 ± 239	>10	>10	>10	>10

[a]Results are expressed as mean±SD calculated from at least 3 experiments each performed in triplicate. Positive controls: URB597 1 μM (FAAH), JZL184 1 μM (MAGL), WWL70 10 μM (ABHD6) and THL 20 μM (ABHD12)

Generally, compounds showed higher affinity for CB2R versus CB1R with a selectivity factor in the range of 1.7-50.7. The only exceptions were the derivatives **B3**, **B4**, **B6** and **C1** that showed a K_i(CB1R)/K_i(CB2R) ratio of 0.86, 0.86, 0.37 and 0.49, respectively. The most potent CB1R/CB2R dual ligand was the 5-bromo derivative **B2** with a K_i value of 2.9 ± 1.2 nM and 1.5 ± 0.8 nM for CB1R and CB2R, respectively. Interestingly, the replacement of the bromine at position 5 with a chlorine atom (compound **B3**) or a fluorine atom (compound **B4**) did not alter CBRs affinity. The presence of a bulkier substituent at position 5, such as a phenyl group (compound **B5**) did not produce any significant alterations of the binding proprieties toward CB2R, while reducing by a factor 30-100 the affinity for CB1R. Instead, the presence of *p*-methoxyphenyl group (**B6**) or *p*-fluorophenyl (**B7**) at position 5 caused a moderate reduction of the binding proprieties at both CBRs. The shift of substituent at the 1-position to the oxygen at the 2- position of the pyridine ring (compound **C1, C2, C6** and **C7**), generally led to a decreased binding affinity mostly for CB1R. Finally, the replacement of the *N*-cycloheptylcarboxamide at position 3 with a *N*-(piperidin-4-yl)carboxamide (**B8**) or with carbohydrates (**B9** and **B10**) dramatically impaired binding properties toward CBRs (K_i values > 10 μM).

Furthermore, the new compounds were tested on the other main components of the ECS, as shown in Table 1, and the obtained results identified interesting polypharmacological properties within the system. In particular, *N*-alkylated derivatives **B5** and **B7** inhibited the main AEA degrading enzyme FAAH with IC_{50} values in the nanomolar range. **B2**, **B3** and **B6** also inhibited AEA hydrolysis with potencies in the low micromolar range. Finally, none of the compounds showed significant inhibition of the major 2-AG hydrolytic enzyme MAGL at the concentration of 10 μM. Similarly, most of the compounds were inactive towards the two minor 2-AG degrading enzymes ABHD6 and ABHD12. The only exceptions were the *N*-substituted compound **B6** and the corresponding *O*-substituted derivative **C6** that showed a moderate potency against ABHD6 with IC_{50} values of 0.53 μM and 0.53 μM, respectively. For ABHD12 only **B7** and **C1** exhibited a moderate inhibition with IC_{50} values of 0.60 μM and 2.12 μM, respectively.

The most potent CBRs ligands **B1-B7**, **C1** and **C2** were tested for their functional activity, using the [^{35}S]GTPγS assay. The results are summarized in Table 2 and showed that compounds unsubstituted at position 5 (**B1**, **C1**) or substituted with a halogen atom (**B2-B4**, **C2**) acted as full agonists at both CBRs. On the contrary, the presence of a bulkier substituent at the same position generated partial agonism, antagonism or inverse agonism at both CBRs. Interestingly, the substitution of a halogen atom at position 5 with a phenyl group (**B5**) switched the dual full agonism at CB1R and CB2R to antagonism at CB1R and inverse agonism at CB2R. The replacement of the phenyl group at position 5 with a *p*-methoxyphenyl (**B6**) group generated antagonism at both CBRs; the replacement with a *p*-fluorobenzyl group (**B7**) generated partial agonism at CB1R and inverse agonism at CB2R. These results indicate that the nature of the substituent at position 5 of the pyridine ring is responsible for the functional activity in accordance to what was previously reported [24,25,32].

Intriguingly, minor modifications of the substituent at position 5 generated three different behaviors at CB2R: full agonism in presence of a bromine atom (**B2**), inverse agonism in presence of a phenyl group (**B5**) and neutral antagonism in presence of a *p*-methoxyphenyl group (**B6**). In order to confirm the uncommon neutral antagonism behavior at CB2R, we performed additional [^{35}S]GTPγS binding assays by competing **B6** with **B2** (agonist) and **B5** (inverse agonist). As shown in Figure 2, pre-incubation of **B6** with increasing concentrations of **B2** resulted in a right-shift of [^{35}S]GTPγS binding curve. As expected by competitive antagonism, E_{max} was not affected, while the potency of **B2** to activate CB2R was significantly reduced, with EC_{50} value that increased by factor 8 in presence of 100 nM **B6**, factor 19 in presence of 300 nM **B6** and factor 70 in presence with 1 μM **B6** (Figure 2A). In another set of experiments, **B6** induced a right-shift also of the [^{35}S]GTPγS binding curve obtained with increasing concentrations of the inverse agonist **B5** (Figure 2B). Interestingly, unlike in presence of the full agonist **B2**, **B6** did not change the potency of **B5** in the [^{35}S]GTPγS binding assay, but rather reduced E_{max} from -49.9% to -28.6% (300 nM) and 24.9% (1 μM), suggesting non-competitive antagonism. The different competition behaviors between **B6** and **B2** (competitive) and **B6** and **B5** (non-competitive) were confirmed by Schild plot (Figure 2C).

Table 2. Functional activity ([^{35}S]GTPγS assay) of compounds **B1-B7**, **C1** and **C2** at CB1R and CB2R.[a]

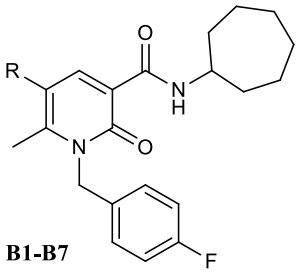

B1-B7

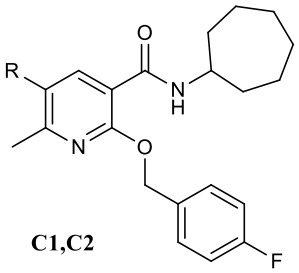

C1,C2

		EC_{50} value (mean ± SD, nM)	
Cmpds	R	CB1R	CB2R
B1	H	40.44 ± 4.00 (Full Ago)	4.15 ± 0.87 (Full Ago)
B2	Br	56.15 ± 49.62 (Full Ago)	11.63 ± 12.74 (Full Ago)
B3	Cl	1.12 ± 9.35 (Full Ago)	3.3 ± 9.51 (Full Ago)
B4	F	43.19 ± 26.20 (Full Ago	24.44 ± 19.97 Full Ago
B5	Phenyl	0.36 ± 18.55 (Antago)	17 ± 16.25 (Inv Ago)
B6	*p*-OCH_3phenyl	270 ± 141.7 (Antago)	170 ± 121.8 Antago
B7	*p*–Fluorophenyl	119.6 ± 111.5 (Part Ago)	6.45 ± 14.4 (Inv Ago)
C1	H	86.15 ± 49.62 (Full Ago)	11.63 ± 10.14 (Full Ago)
C2	Br	586.15 ± 59.60 (Full Ago)	31.63 ± 20.74 (Full Ago)

[a]In brackets the behavior on CB1R and CB2R is reported from the [^{35}S]GTPγS assay: Part Ago: partial agonist; Full Ago: full agonist; Inv Ago: inverse agonist; Antago: antagonist. Positive controls: CP55,940 100 nM as CB1R and CB2R agonist (full), SR141617A 1 μM as CB1R inverse agonist and AM630 1 μM as CB2R inverse agonist.

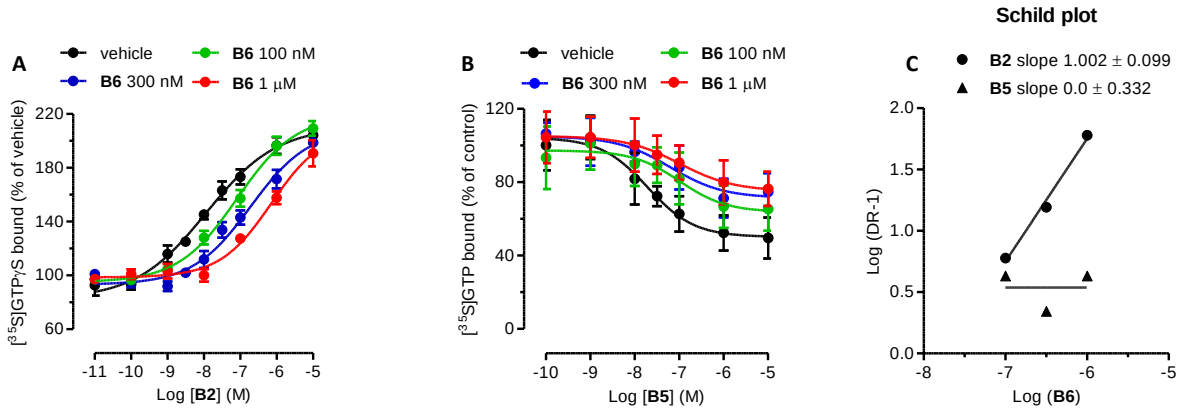

B6 (nM)	EC_{50} value 95% CI, nM)	Emax (95% CI, nM)
0	11.6 (4.4 - 30.7)	210 (194 - 227)
100	81.20* (36.2 - 182.3)	219 (200 - 237)
300	191.7** (55.4 - 663.1)	209 (200 - 238)
1000	710.6** (149.8 - 3371)	208 (187 - 242)

B6 (nM)	EC_{50} value (95% CI, nM)	Emax (95% CI, nM)
0	19.4 (9.8 - 38.2)	-49.9 (-55.6 - -44.1)
100	102.4 (20.1 - 500.3)	- 36.3 (-47.5 - -25.0)
300	62.4 (14.4 - 270.4)	-28.6** (-37.6 - -19.5)
1000	102.8 (16.8 - 656.4)	-24.9** (-26.4 - -13.3)

Figure 2. Pre-incubation of neutral antagonist **B6** concentration-dependently reduces (A) **B2** (full agonist) potency to activate CB2R in [^{35}S]GTPγS assays without modifying E_{max}. (B) **B6**-induced concentration-dependent reduction of E_{max} in the [^{35}S]GTPγS binding curve obtained with the inverse agonist **B5**, without affecting potency. (C) Schild plot analysis derived from data in A) and B) confirmed competitive behaviors between **B2** and **B6** and non-competitive behavior between **B5** and **B6**. Table under graphs in A) and B) summarize EC_{50} values and E_{max} (mean plus 95% CI) calculated from the curved in presence of different concentrations of **B6**. CP55,940 100 nM was used as positive control as CB2R agonist (full) and AM630 1 μM as CB2R inverse agonist. Data in graphs show mean values ± SEM of at least three independent experiments, each performed in triplicate. *$p < 0.05$, **$p < 0.01$ vs. vehicle (two-tailed student t-test).

2.3. In silico ADME profiling

Compounds **B1-4** and **C1-2**, which showed to be the most active agonist compounds, were subjected to a preliminary *in silico* ADME profiling using the swiss ADME web tool [40] as previously performed [41,42].

The octanol/water partition coefficient (expressed as logP), which is commonly used as an indicator of molecular lipophilicity, and the aqueous solubility (expressed as logS) of the compounds were predicted using a consensus strategy, i.e. combining the five logP and the three logS calculation methods respectively available in the web tool, while gastrointestinal absorption and blood-brain barrier permeation were estimated by swiss ADME based on the calculated logP and topological polar surface area of the compounds. Table 3 reports the physicochemical properties as well as the Lipinski rules violations, calculated for the selected compounds. Due to their lipophilic nature, low values of logS and high values of logP were predicted for the ligands. Nevertheless, all compounds satisfied the Lipinski's rule of five and showed logP and logS values comprised within the range of 95% of known drugs, with the only exception of compound **C2** that showed a logS slightly outside the range ($-6.5 < \log S < 0.5$). Moreover, all ligands were predicted to be easily absorbed in the gastrointestinal tract and to permeate the blood-brain barrier. As expected, the calculated properties highlighted the higher hydrophobic character of the analogues with a bromine and chlorine atom at position 5 of the central scaffold with respect to those with a hydrogen and fluorine atom at the same position. In fact, compounds **B2** and **C2** showed higher logP and lower logS values than **B1** and **C1**, respectively. Interestingly, the central scaffold of the compounds seems to appreciably influence their physicochemical properties, since **C1** and **C2** bearing an alkoxypyridine core were predicted to be more lipophilic with respect to their structural isomers **B1** and **B2**, respectively.

Table 3. Predicted lipophilicity (logP), water solubility (logS), Caco-2 and MDCK cell apparent permeability, as well as rules violation of new ligands.

Cmpds	Cons. logP	Cons. logS	GI absorption	BBB permeation	RoF[a] violations
B1	4.0	-5.4	high	yes	0
B2	4.5	-6.0	high	yes	0
B3	4.4	-5.8	high	yes	0
B4	4.2	-5.4	high	yes	0
C1	4.3	-5.9	high	yes	0
C2	5.0	-6.7	high	yes	0

[a]Lipinski rule of Five.

2.4. Molecular modeling studies

Based on activity profile on the targets of ECS and *in silico ADME* properties, derivative **B2** was selected as the most promising compound with orthosteric agonist activity on both CBRs. A docking study refined by energy minimization was performed for compound **B2** into CB1R and CB2R binding site in order to rationalize the experimental results obtained from the biological evaluation. For this study, the ligand was docked using AUTODOCK 4.2 into the X-ray structure of human CB1R in complex with AM11542 (PDB code 5XRA) [43] and the recently deposited crystal structure of human CB2R in complex with AM10357 (PDB code 5ZTY) [44]. In each docking calculation, a total of 200 different docking solutions were generated and clustered using an RMSD cut-off of 2.0 Å. The best docking pose generated in each receptor was selected and the corresponding ligand-protein complex was then energy minimized using AMBER16 to optimize the binding mode of the ligand (See Materials and Methods for details). Figure 3A shows the final binding disposition of compound **B2** into CB2R. The ligand predominantly interacts with the four

transmembrane domains (TM) of the receptor TM 2, 3, 6 and 7, among which the central 1,2-dihydro-2-oxo-pyridine core and the cycloheptyl carboxamide group of the compound are located, forming multiple hydrophobic interactions. In particular, the core ring of the ligand shows a T-shaped stacking with F183 and additional lipophilic contacts with F87, F117, V113 and M265. The 5-bromine substituent is inserted in a pocket formed by V261, M265, F281, S285 and C288 that seems not wide enough to well tolerate bulkier groups, which may explain the reduced activity and/or the different functional profile of compounds **B5-7** bearing bigger aromatic moieties at position 5, with respect to **B2**. The carboxamide group of the ligand shows aromatic interactions with F87 and forms an intramolecular H-bond with the carbonyl oxygen of the core ring, while the cycloheptyl ring is placed into a lipophilic pocket mainly delimited by F87, F91, F94, I110 and P184. The disposition of this group is consistent with the experimental results highlighting a complete loss of activity for compounds **B8-10**, bearing remarkably polar moieties in place of the cycloheptyl ring. Finally, the *p*-fluorobenzyl group of **B2** well fits another hydrophobic pocket located among TM 3-5. Precisely, this portion of the ligand forms π-π stacking with F183 and W194 as well as lipophilic interactions with all other residues delimiting the pocket and in particular with T114, I186, L191 and M265. It is reasonable to hypothesize that compounds **C1** and **C2** present a binding mode similar to that predicted for **B2**, with their *p*-fluorobenzyloxy moiety placed in the same pocket occupied by the *p*-fluorobenzyl group of **B2**. This would be consistent with the full agonist activity observed for both **B2** and **C1** and **C2**. However, the presence of the side chain of L110, which is placed in the proximity of the piridone oxygen of **B2**, could sterically hamper an optimal disposition of the *p*-fluorobenzyloxy moiety of compounds **C1** and **C2**, thus justifying their reduced activity with respect to **B2**. Finally, the complete loss of activity of **C6** and **C7** could be due to the additionally negative effect of their large substituents in

position 5, which may also endow these ligands with a different effect on CBRs, as observed for **B5**-**B7**. As shown in Figure 3B, the ligand was predicted to adopt a binding mode into CB1R that is very similar to that observed into CB2R. In fact, the different structural portions of the compound are localized in the same subpockets of the receptor and fundamentally show the same interactions with the protein residues. This is consistent with the comparable affinity of **B2** for both CB1R and CB2R. The only difference between the binding mode of the ligand into the two receptors consists in a small adjustment of its disposition and a rotation of the cycloheptyl group, which are probably due to the presence of L193 and L359 in CB1R in place of the homolog residues I110 and V261 of CB2R that slightly change the shape of the binding site. Accordingly, the considerations about the SAR data of the series of ligands in relation to the binding mode of **B2** into CB2R could be also extended to CB1R.

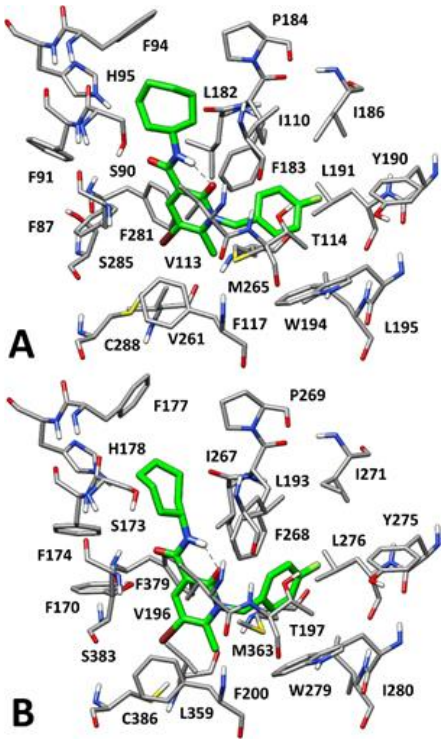

Figure 3. Predicted binding mode of compound **B2** into CB2R (A) and CB1R (B) binding sites.

*2.5. Effect of **B2** on CB2-mediated release of ILs from LPS- stimulated BV-2 Microglial Cell*

In order to evaluate *in vitro* CB2R-mediated anti-inflammatory effect of **B2**, microglial cells BV-2 were stimulated with LPS to induce an inflammatory response [45-49]. LPS stimulation has been widely used to activate microglial cells and promote interleukin release [50,51]. As a marker of inflammatory response, we quantified the levels of extracellular-released interleukins in activated BV-2 cells treated either with **B2** alone or in presence with the CB2R antagonist SR144528.

LPS stimulation significantly increased the release of the pro-inflammatory interleukins IL-1β and IL-6 (734.3 ± 35.1% and 764.7 ± 22.9%) (Figures 4A and 4B) as compared to non-stimulated cells (NC). On the contrary, no significant change in the release of the anti-inflammatory interleukin IL-10 (Figure 4C), was detected after LPS-stimulation.

In LPS-activated BV-2 cells, **B2** significantly decreased the secretion of IL-1β (Figure 4A) and IL-6 (Figure 4B). In detail, compared to untreated LPS-stimulated cells, the secretion of IL-1β was reduced to 24.6 ± 7.3% after treatment with 10 μM **B2**. In addition, the release of IL-6 was decreased to 27.8 ± 1.5% after treatment with 10 μM **B2**. According to an anti-inflammatory effect, **B2** increased the release of anti-inflammatory IL-10 to 483.7 ± 76.5% as compared to untreated LPS-stimulated cells (Figure 4C).

Overall, the ability of **B2** to modulate the secretion of pro- and anti-inflammatory ILs was comparable to the ability of the classic CB2R agonist JWH-133 (Figures 4A-C). The pre-treatment with the selective CB2R antagonist SR144528, which *per se* did not modify IL release, fully counteracted the changes induced by **B2** on pro- and anti-inflammatory ILs release (Figures 4A-C), supporting a CB2R-mediated anti-inflammatory effect of **B2**.

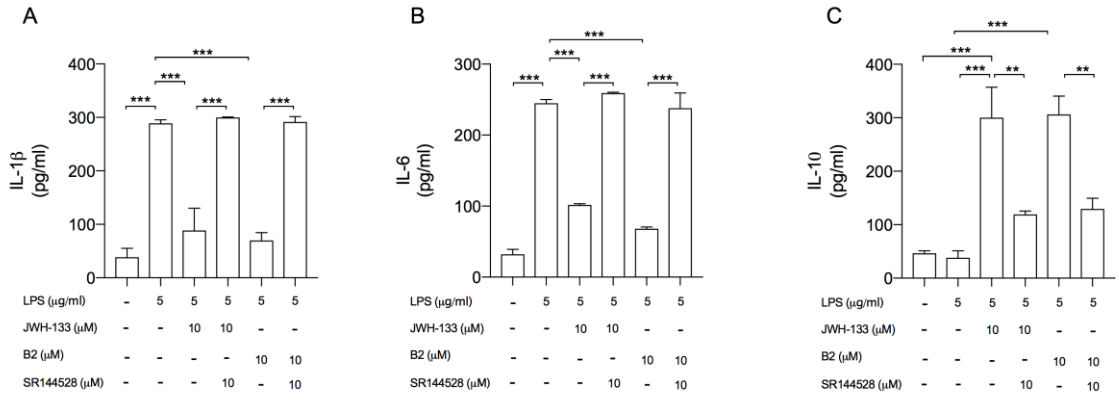

Figure 4. B2 decreased the inflammatory response by the modulation of CB2R on LPS-stimulated BV2 microglial cells. **B2** decreased the release of pro-inflammatory IL-1β (A) and IL-6 (B) and increased the release of anti-inflammatory IL-10 (C), in a comparable manner to the classic CB2R agonist JWH133. The CB2R antagonist SR144528 counteracted the **B2** anti-inflammatory effects (A, B, C). Bars represent the release of ILs (pg/ml) in presence of the compounds at the indicated concentrations. BV-2 microglial cells were pre-treated with **B2** for 30 minutes and then stimulated with LPS (5 μg/ml) for 4h. In case of co-administration with SR144528, this latter was administered 15 minutes before the agonist. Data are the mean ± SEM (bars) of three independent experiments each performed in duplicate. *p<0.05, **p<0.01 and ***p<0.001 between two selected bars–ordinary one-way ANOVA followed by Bonferroni's multiple comparison test.

*2.6. Effect of **B2** on the glutamate release*

To evaluate the effect of **B2** on the glutamate release, nerve terminals (synaptosomes) were isolated from the rat hippocampus and endogenous glutamate efflux was measured in superfusion. The technique allows the activity evaluation of the novel compound on the CBRs on glutamatergic nerve ending, preventing indirect effects at post-synaptic level or on glial cells.

In preliminary experiments, we used ACEA as positive control CB1R agonist and we found that the 4-aminopyridine(4-AP)-evoked release of glutamate was partially inhibited by CB1R agonism, in accordance to literature [52]. In fact, the CB1R agonist ACEA (10 μM), inhibited 4-AP-evoked glutamate release (600 μM, 2 min; Figure 5A). The CB1R antagonist SR141716A (1 μM), abolished the inhibitory action of ACEA on 4-AP evoked glutamate release. The CB2R antagonist, SR144528 (1μM) did not affect the ACEA-mediated inhibition of 4-AP evoked glutamate release. SR141716A and SR144528 at the used concentrations did not affect neither basal nor 4-AP-evoked endogenous glutamate release. Moreover, ACEA at the used concentrations did not affect the basal efflux. The concentrations for 4-AP, CB1R agonist and antagonist, and the CB2R antagonist, were chosen according to the literature [52-54].

These data indicate that: 1) CB1R is present and functional on glutamatergic hippocampal presynaptic nerve terminals, as previously reported [52-54]; 2) the CB1R agonist ACEA, at the used concentration, is able to inhibit the depolarization-evoked glutamate release without the involvement of CB2R.

The effect of **B2** was assessed in the same experimental conditions. At the concentrations of 10 μM, **B2** inhibited 4-AP-evoked glutamate release (Figure 5B), while at 1 μM it induced a moderate not statistically significant effect. The CB1R antagonist SR141716A (1 μM and 3 μM), prevented the inhibitory action of **B2** (10 μM). On the contrary, the CB2R antagonist SR144528 (1μM) did not affect the **B2**-mediated inhibition of 4-AP evoked glutamate efflux. Therefore, **B2** mimicked the positive control CB1R agonist in modulating glutamate release.

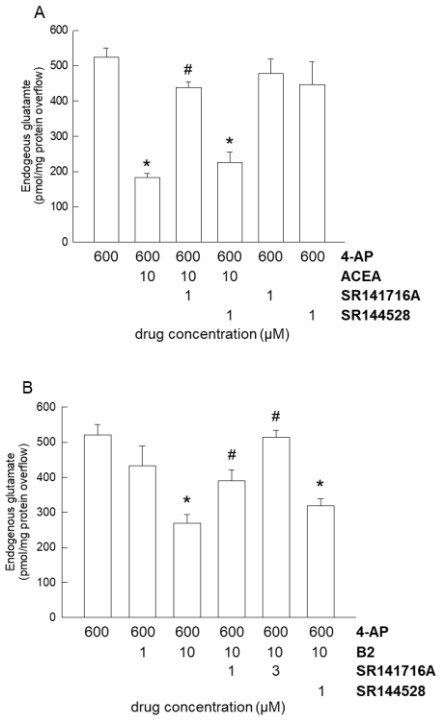

Figure 5. Activation of CB1R inhibited the evoked glutamate release from hippocampal nerve terminals in superfusion experiments. A) The CB1R agonist ACEA inhibited the 4-AP-evoked efflux of endogenous glutamate which was prevented by SR141716A (CB1R antagonist). B) Pharmacological characterization of the effect of **B2**: inhibition of 4-AP-evoked efflux of endogenous glutamate, which was prevented by CB1R antagonism with SR141716A. Bars represent the overflow (pmol/mg protein) of endogenous glutamate in the presence of the drugs at the indicated concentrations. 4-AP was added (2 min) during superfusion: ACEA, SR141716A, and **B2** were added starting 8 min before the depolarizing stimulus. Data are the mean ± SEM (bars) of n= 3-9 experiments each performed in triplicate. *p<0.05 compared with the effect of 4-AP; #p<0.05 compared with the effect of ACEA in panel A and **B2** 10 μM in panel B (Mann-Whitney test to compare selected pairs of columns).

*2.7. Effects of **B2** against Neuropathic Pain in mice*

The selected compound **B2** was tested against neuropathic pain in a mouse model of chemotherapy-induced neuropathy. The repeated administrations of the anticancer drug oxaliplatin was able to decrease the pain threshold when measured by applying a cold non noxious stimulus (cold plate test), a measurement representative of the clinical condition of cold allodynia [55,56]. The acute administration (*per os*) of **B2** dose-dependently (5 – 50 mg.kg^{-1}) relieved neuropathic pain starting from the dose of 5 mg.kg^{-1}. Efficacy onset and duration ranged between 15 and 60 min after treatment (Figure 6). Efficacy and potency were comparable to that of well known pain relieving drugs (pregabalin and duloxetine) in the same model [55]. Furthermore, the pharmacodynamic mechanism of the anti-neuropathic effect of **B2** was studied by using selective antagonists of the CB1R and CB2R, respectively. When co-administered, both the CB1R antagonist SR141716A and the CB2R antagonist SR144528 were able to fully prevent the pain relieving effect of **B2**. A double stimulation of CB1R and CB2R is then suggested for **B2** (Figure 6).

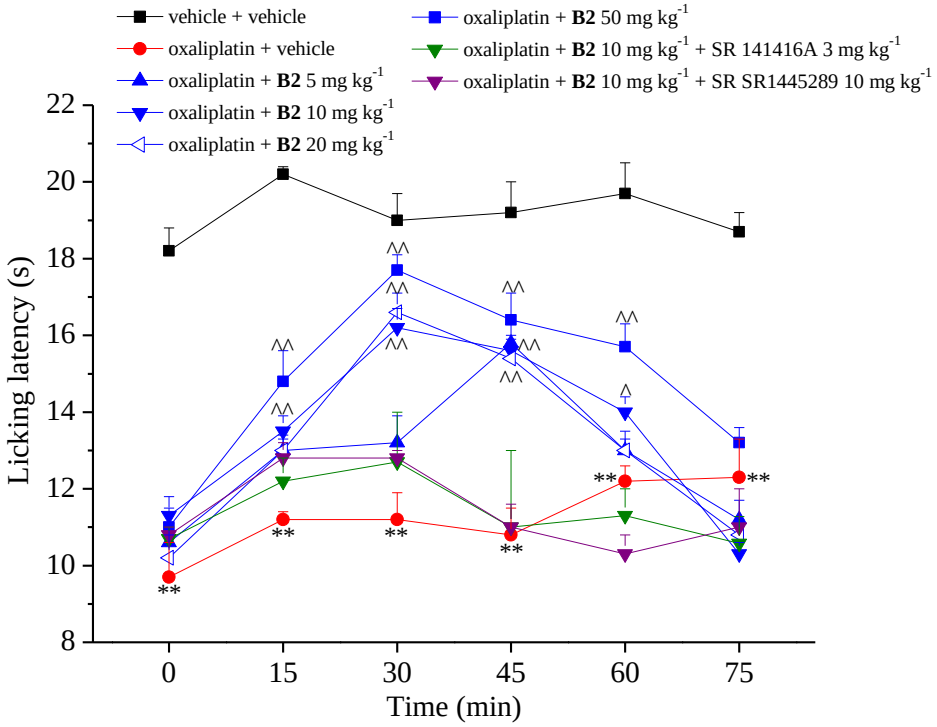

Figure 6. Neuropathic pain modulation by **B2**. Effects were evaluated in a mouse model of neuropathic induced by oxaliplatin (2.4 $mg.kg^{-1}$, by intraperitoneal route, repeatedly). The pain threshold was measured by the Cold plate test evaluating the first behavioural response (licking latency) to a cold non noxious stimulus. Results are reported as mean ± SEM of 10 mice analyzed in 2 different experimental sessions. **P<0.01 vs vehicle + vehicle; ^P<0.05 and ^^P<0.01 vs oxaliplatin + vehicle.

2.8. Effect of B2 on EAE model of multiple sclerosis

B2 was tested in the EAE mouse model of multiple sclerosis. Mice were treated for 20 days with **B2** at the dose of 10 $mg.kg^{-1}$ (daily, i.p.) which was chosen as the lowest dose to elicit full pharmacological effect in the oxaliplatin-induced neuropathic pain model. EAE mice treated with **B2** showed a significant improvement of clinical score as compared to vehicle-treated littermates (Figure 7). **B2** significantly improved disease severity both in the initial (day 2 to day 4) and later stage (day 10 to day 19) of the disease (Figure 7A), resulting in an overall reduction of disease severity over 20 days of treatment (Figure 7B) and showed a tendency to reduce the frequency of cases achieving a high disease severity (clinical score ≥ 2), as compared to vehicle-treated mice (Figure 7C). In the initial phase, **B2** induced a milder reduction (30%) of clinical score only at day 2, 3 and 4 post-treatment. In the second phase of the disease, the compounds elicited a more pronounced reduction (50-60%) of clinical score that lasted for 9 days (from day 10 to day 19) (Figure 7A).

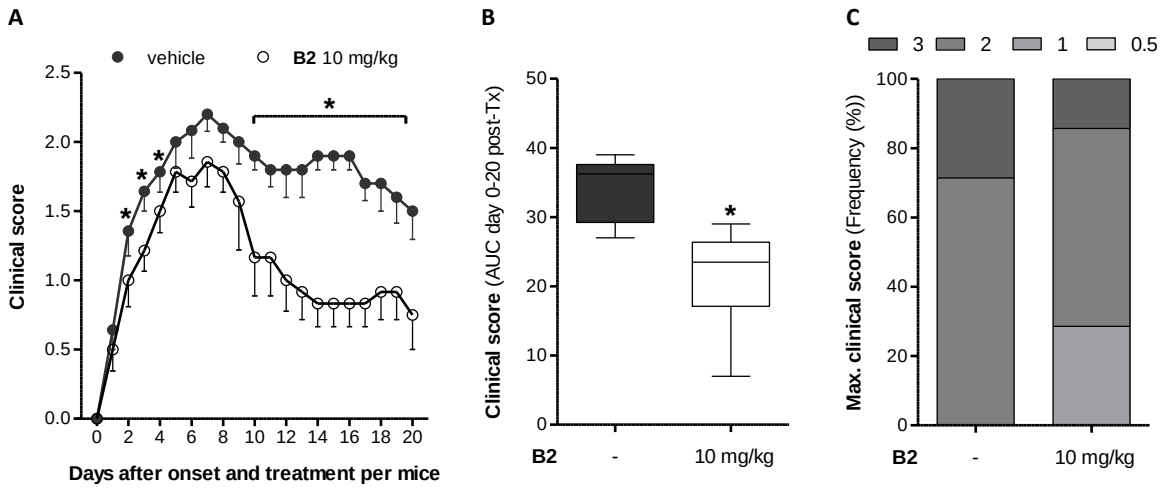

Figure 7. Clinical evaluation of EAE mice chronically treated with **B2**. Disease onset was observed between day 10 and day 16 after immunization and daily treatments (i.p.) with vehicle (DMSO) or 10 mg.kg^{-1} **B2** started individually on the day of onset of each mouse and lasted for 20 days. A) Time course of disease severity, evaluated using a 3-points clinical score. The day of onset is considered as day 1. Data shows mean ± SEM, statistical differences were evaluated using multiple *t* test corrected by the Holm-Sidak method. B) Cumulative disease severity, calculated as the area under the curve (AUC) from day 0 to day 20. Data shows a boxplot with min and max values, statistical differences were evaluated with the Mann-Whitney test. C) Frequency of the maximal clinical scores observed within each group. Data shows cumulative frequency in %, statistical differences were evaluated with Chi-square and Fisher's exact test. *, $p < 0.05$; n = 7 mice per group.

Based on its dual agonism at CB1R and CB2R, we can speculate that the initial improvement of disease severity induced by **B2** is mostly linked to CB1R activation possibly by reducing excessive glutamate release (excitotoxicity). In the second phase, **B2** can exert more pronounced and long-lasting effects by counteracting neuroinflammation *via* CB2R activation. This hypothesis is indirectly supported by our data showing that **B2** reduced glutamate release in isolated

synaptosomes *via* CB1R activation (Figure 5) and reduced neuropathic pain (which has an inflammatory component) *in vivo via* CB1R and CB2R activation (Figure 6). In addition, based on *in vitro* data we cannot exclude a minor contribution of FAAH inhibition.

Finally, the loss of improvement in disease severity between day 5 and day 9 can be attributed to desensitization of CB1R in the brain. In the first 4 days of treatment, **B2**-treated mice showed the typical (transitory) post-administration CB1R-dependent reduction in locomotion, in body temperature and catalepsy-like behaviour as part of the tetrad [57], (see next paragraph for full tetrad). On the contrary, after the fifth day of administration, this signs of CB1R activation in the brain disappeared. Our observation is partially confirmed by the reduction of functional CB1R in brain ([^{35}S]GTPγS assay) of mice treated for 20 days with **B2** as compared to vehicle (Figure S1 in Supporting Information).

2.8.1 Tetrad test.

To confirm CB1R activation in the brain, **B2** was tested in a battery of four phenotypic tests to assess body temperature, locomotion, nociception and catalepsy-like behaviour (collectively referred as "tetrad") [57]. The full tetrad is a well-established readout of central CB1R activation in rodents and it is validated by phytocannabinoid (e.g. Δ9-THC) [58] and synthetic CB1R agonists (e.g. WIN55,212) [59]. After single administration, **B2** at the dose of 5 mg.kg^{-1} (i.p.) elicited the full tetrad in BALB/c mice by lowering body temperature (Figure, 8A), reducing spontaneous locomotion (Figure 8B), increasing immobility time (Figure 8C) and inducing analgesia (Figure 8D). These data indicate that **B2** can diffuse across the blood-brain-barrier and reaches bioactive concentration in the brain. In order to validate the specific CB1R activation by **B2**, two related compounds (**B5** and **B6**), that behave as potent CB1R antagonists (Table 2), were tested. In line

with the results *in vitro* (Table 2), 5-phenyl (**B5**) and 5-*p*-methoxyphenyl (**B6**) derivatives did not elicit the tetrad. These data confirm the specific activation of CB1R *in vitro* and *in vivo* of **B2** as compared to other related compounds.

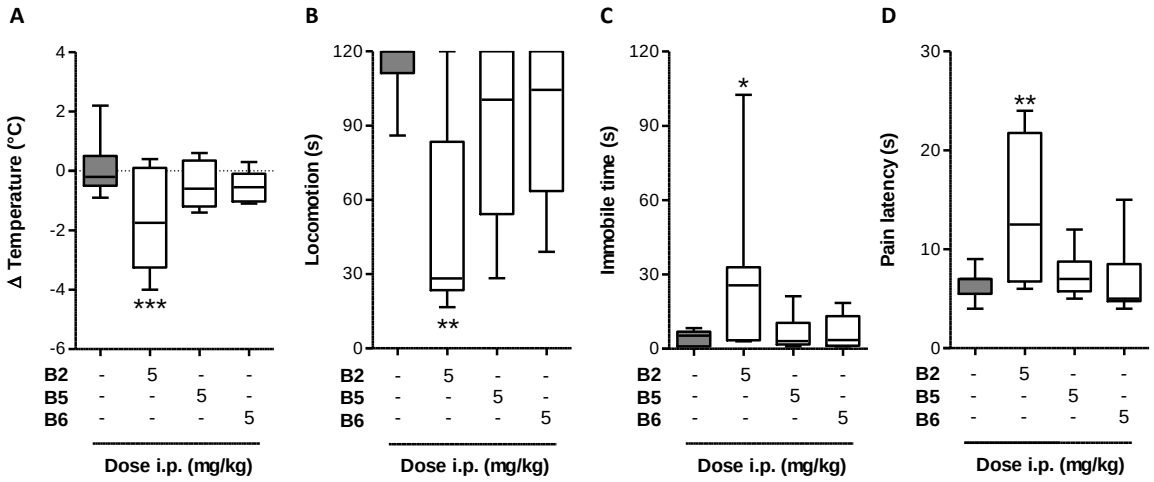

Figure 8. Tetrad test. **B2**-induced hypothermia (A), hypolocomotion (B), catalepsy-like behaviour (C), and analgesia (D) in BALB/c mice. The tetrad was assessed after 1 h from i.p. injection of **B2**, **B5** and **B6** at the dose of 5 mg.kg^{-1}. The data show Whiskers min to max values. Groups were compared with vehicle treated control group using a one-way ANOVA after Tukey's post hoc test or unpaired *t* test. n = 5–20 mice per group. *p< 0.05; **p<0.01; ***P<0.001.

3. CONCLUSION

Here, we report the synthesis of a new series of 1,2-dihydro-2-oxo-pyridine-3-carboxamide derivatives and the characterization of their biological activity *in vitro* and *in vivo*. Our data indicate that small modifications on the chemical scaffold can lead to interesting multi-target pharmacological profiles in the ECS. For example, through minor modifications of the substituent at position 5 we could identify three distinct functional effects at CB2R, full agonism (**B2**), inverse agonism (**B5**) and an uncommon behavior as neutral antagonism (**B6**). In particular, we

characterized the pharmacological effects of compound **B2**, a potent dual CB1R/CB2R agonist with good drug-like properties.

The activity of **B2** on neuroinflammation and excitotoxic damage by excessive glutamate release, that are the two pivotal pathogenic mechanisms of MS, were performed in *in vitro* assays. **B2** reduced LPS-induced activation of microglial cells in a CB2R-depended manner by decreasing secretion of pro-inflammatory cytokines (IL-1β and IL-6), while enhancing the anti-inflammatory cytokine (IL-10), in line with the reported ability of CB2R to counteract microglia activation, reducing the inflammatory process [50, 60-65]. In another set of experiments, **B2** reduced the depolarization-evoked glutamate release in nerve terminals isolated from rat hippocampus in a CB1R-dependent manner.

In vivo, **B2** showed potent CB1R- and CB2R-dependent antinociceptive effect upon oral administration in a mouse model of oxaliplatin-induced neuropathic pain, which is a common symptom in MS patients. To note, Δ9-THC was not able to reduce hypersensitivity in the same oxaliplatin model [66], the potent mixed CB1R/CB2R agonist WIN55,212 attenuated neuropathic pain induced by other neurotoxic anticancer agents (paclitaxel and vincristine) [67,68], through both receptor mechanisms but efficacy findings against oxaliplatin-induced neuropathy are still lacking. In an EAE mouse model of multiple sclerosis, **B2** showed significant improvement of disease severity both in the earlier and later phase of the disease. Based on our data on glutamate release and microglial activation, we can speculate that **B2** exerted positive effect in the EAE model *via* CB1R-mediated reduction of excitotoxicity and CB2R-mediated anti-inflammatory effect. CB1R-activation in brain is supported by the full tetrad, which is a clear read-out of CB1R activation in the CNS. Given these data, the new ECS multi-target modulator **B2**, could represent

a valuable tool compound for future development of novel therapeutic strategies to control symptoms and disease progression in MS.

4. EXPERIMENTAL

4.1. Chemistry

Commercially available reagents were purchased from Sigma Aldrich, Alfa Aesar or Tokio Chemical Industry and used without purification. ^{1}H NMR and ^{13}C NMR were recorded at 400 and 100 MHz respectively, on a Bruker AVANCE III^{TM} 400 spectrometer or with a Bruker Avance II instrument operating at 250.13MHz (^{1}H) and 62.9 MHz (^{13}C). Chemical shifts (δ) are reported in parts per million related to the residual solvent signal, while coupling constants (*J*) are expressed in Hertz (Hz). Microwave-assisted reactions were run in a Biotage® microwave synthesizer. All final compounds were analyzed by HPLC, showing a purity ≥ 95%. A Beckman HPLC instrument equipped with a System Gold Solvent Delivery module (Pumps) 125, System Gold UV/VIS Detector 166, Detector set to 278 nm, was employed. Analyses were performed on a reverse phase C18 column (Phenomenex 250 × 4.6 mm, 5 mm particle size, Gemini). The mobile phase was constituted by a mixture of H_2O/AcOH (0.1% v/v) (eluent A) and ACN (eluent B). A gradient starting from 50% of B, changing to 100% of B over 20 min, and returning to the initial conditions over 10 min, was used for compounds. The flow rate was 1.0 ml/min. High-resolution mass spectra (HRMS) were recorded on a Q Exactive™ Plus Hybrid Quadrupole-Orbitrap™ Mass Spectrometer (Thermo Fisher Scientific), resolution 140,000 at m/z 200. Organic solutions were dried over anhydrous Na_2SO_4 or $MgSO_4$. Evaporation was carried out *in vacuo* using a rotating evaporator. Kieselgel 60 (E. Merck, 70–230 and 230–400 mesh, respectively) was used for column and flash chromatography. Some of flash chromatography were conducted by the automated

system Isolera Four SVTM (Biotage®), equipped with UV detector with variable wavelength (200-400 nm). Reactions were monitored by TLC on Kieselgel 60 F_{254} ((E. Merck) with detection by UV light (λ = 254 nm)) and/or with ethanolic 10% phosphomolybdic or sulfuric acid, and heating. All reactions involving air- or moisture-sensitive reagents were performed under an argon or nitrogen atmosphere using anhydrous solvents. Dried solvents were obtained by distillation according to standard procedure [69] and stored over 4Å molecular sieves activated. Melting points were determined on a Kofler hot-stage apparatus and are uncorrected.

*4.1.1. N-Cycloheptyl-1,2-dihydro-6-methyl-2-oxo-pyridine-3-carboxamide (**1**).*

A solution of 1,2-dihydro-6-methyl-2-oxo-pyridine-3-carboxilyc acid (500.0 mg, 3.27 mmol) in anhydrous DMF (8.1 mL) was stirred in an ice-bath. TBTU (1.26 g, 3.92 mmol) and triethylamine (1.2 mL, 9.16 mmol) were added at 0 °C. After 30 minutes, cycloheptylamine (0.4 mL, 3.27 mmol) was added and the reaction contents were stirred at 0°C for 30 minutes and then at room temperature for 12 h. After removing the solvent under reduced pressure, the reaction mixture was dissolved in $CHCl_3$ and washed with water. The organic phase was dried over anhydrous Na_2SO_4, filtered and evaporated under reduced pressure. The purification by flash chromatography on silica gel (ethyl acetate/petroleum ether 8:2) lead to the isolation of the pure amide (554.0 mg, 2.24 mmol). **1**: Yield 69%. ^{1}H NMR ($CDCl_3$, 400 MHz) δ: 13.11 (bs, 1H, OH), 9.63 (bd, 1H, *J* = 7.6 Hz, NH), 8.52 (d, 1H, *J* = 7.4 Hz, H_4-Py), 6.34 (d, 1H, *J* = 7.4 Hz, H_5-Py), 4.20 (m, 1H, CHN), 2.44 (s, 3H, C*H*$_3$-Py), 1.76 (m, 12H, 6×CH_2). ^{13}C NMR ($CDCl_3$, 100 MHz) δ: (ppm) 164.64, 162.68 (2×C=O), 149.26 (*C*$_6$-Py), 145.51 (*C*$_4$-Py), 118.51 (*C*$_3$-Py), 107.91 (*C*$_5$-Py), 49.96 (CH-NH), 34.98 (2×*C*H_2CHNH), 28.33 (2×CH_2), 24.14 (2×CH_2), 19.09 (CH_3-Py).

*4.1.2. N-Cycloheptyl -1,2-dihydro-5-bromo -6-methyl-2-oxo-pyridine-3-carboxamide (**2**).*

N-Cycloheptyl-1,2-dihydro-6-methyl-2-oxo-pyridine-3-carboxamide **1** (646.0 mg, 2.60 mmol) was dissolved in $CHCl_3$ (4.3 mL) and a solution of bromine (0.1 mL, 312.0 mg, 2.60 mmol) in $CHCl_3$ (2.6 mL) was added dropwise. The reaction mixture was stirred at room temperature for 12 h and then diluted with $CHCl_3$. The solution was treated with a saturated solution of sodium thiosulfate and then was washed with water. The organic phase was dried over anhydrous Na_2SO_4, filtered and evaporated under reduced pressure, affording compound **2** (665.0 mg, 2.00 mmol) as a yellow solid, which was used in the next step without further purification. **2**: Yield 77%. ^{1}H NMR ($CDCl_3$, 400 MHz) δ: 13.39 (bs, 1H, OH), 9.44 (bd, 1H, J = 7.3 Hz, NH), 8.65 (s, 1H, H_4-Py), 4.21 (m, 1H, CHN), 2.53 (s, 3H, CH_3-Py), 1.78 (m, 12H, 6×CH_2). ^{13}C NMR ($CDCl_3$, 100 MHz) δ: (ppm) 163.59, 161.29 (2×C=O), 148.38 (C_6-Py), 147.87 (C_4-Py), 119.89 (C_3-Py), 101.77 (C_5-Py), 50.03 (CH-NH), 34.81 (2×$C$$H_2$CHNH), 28.24 (2×$CH_2$), 23.96 (2×$CH_2$), 19.77 ($CH_3$-Py).

*4.1.3. N-Cycloheptyl-1,2-dihydro-5-chloro-6-methyl-2-oxo-pyridine-3-carboxamide (**3**).*

N-Chlorosuccinimmide (270.0 mg, 2.01 mmol) was slowly added to a suspension of *N*-cycloheptyl-2-oxo-pyridine-3-carboxamide **1** (500.0 mg, 2.01 mmol) in acetonitrile (6.0 mL) at room temperature and the reaction was refluxed for 3 h. After cooling to room temperature, the reaction was quenched with water and repeatedly extracted with ethyl acetate. The organic phases were collected, dried over Na_2SO_4, filtered and evaporated under reduced pressure to afford compound **3** (358.0 mg, 1.27 mmol), which was used in the next step without further purification. **3**: Yield 63%. ^{1}H NMR ($CDCl_3$, 400 MHz) δ: 13.26 (bs, 1H, OH), 9.53 (s, 1H, H_4-Py), 9.43 (bd,

1H, *J* = 7.8 Hz, NH), 4.23 (m, 1H, CHN), 2.47 (s, 3H, C*H*$_3$-Py), 1.91 (m, 2H, CH_2), 1.66 (m, 10H, 5×CH_2).

*4.1.4. N-Cycloheptyl-1,2-dihydro-5-fluoro-6-methyl-2-oxo-pyridine-3-carboxamide (**4**).*

1-Chloromethyl-4-fluoro-1,4-diazoniabicyclo[2.2.2]octanebis(tetrafluoroborate) (1.10 g, 2.83 mmol) was added in one portion to a suspension of the 2-oxo-pyridine-3-carboxamide **1** (680.0 mg, 2.83 mmol) in acetonitrile (5.6 mL) at room temperature and the mixture was refluxed for 12 h. After cooling to room temperature, the solvent was removed under reduced pressure. The residue obtained was dissolved in ethyl acetate, washed with water. The organic phase was then dried over anhydrous Na_2SO_4, filtered and evaporated under reduced pressure to obtain a yellow oil which was then purified by flash chromatography on silica gel (1:1 ethyl acetate/petroleum ether) affording compound **4** (121.0 mg, 0.45 mmol). **4**: Yield 16%. ^{1}H NMR ($CDCl_3$, 400 MHz) δ: 13.18 (bs, 1H, OH), 9.58 (bd, 1H, *J* = 7.8 Hz, NH), 8.47 (d, 1H, $J_{H,F}$= 9.2 Hz, H_4-Py), 4.20 (m, 1H, C*H*N), 2.44 (s, 3H, C*H*$_3$-Py), 1.94 (m, 2H, CH_2), 1.70 (m, 10H, 5×CH_2). ^{19}F NMR ($CDCl_3$, 400 MHz) δ: 146.52.

*4.1.5. General procedure for the synthesis of 5-substituted 3-carboxamide derivatives **5-7***

A mixture of PPh_3 (163.0 mg, 0.62 mmol) and $Pd(OAc)_2$ (27.0 mg, 0.12 mmol) in 1.7 mL of anhydrous 1,4-dioxane was stirred at room temperature under nitrogen flux. After 15 minutes, the 5-bromo derivative **2** (406.0 mg, 1.24 mmol) was added followed by 2.0 M sodium carbonate aqueous solution (2.4 mL), methanol (2.4 mL) and the suitable arylboronic acid (2.48 mmol). The mixture was heated in a microwave reactor at 110 °C for 1h (power 200 W, pressure 100 psi, stirring on). After cooling, the reaction mixture was filtered under vacuum using celite, evaporated

under reduced pressure, treated with water and extracted with $CHCl_3$. Combined organic layers were dried over anhydrous Na_2SO_4, filtered and evaporated under reduced pressure, to obtain a residue which was purified by flash chromatography.

*4.1.5.1. N-Cycloheptyl-1,2-dihydro-5-phenyl-6-methyl-2-oxo-pyridine-3-carboxamide (**5**).*

Compound 5 was prepared using phenylboronic acid and it was purified by flash chromatography on silica gel (7:3 *n*-hexane/ethyl acetate). **5**: Yield 67%. ^{1}H NMR (400 MHz, $CDCl_3$) δ: 13.12 (bs, 1H, OH), 9.72 (bd, 1H, *J* = 7.6 Hz, NH), 8.57 (s, 1H, H_4-Py), 7.28 (m, 5H, Ar-*H*), 4.25 (m, 1H, CHN), 2.47 (s, 3H, C*H*$_3$-Py), 1.68 (m, 12H, 6×C*H*$_2$).

*4.1.5.2. N-Cycloheptyl-1,2-dihydro-5-(4-methoxyphenyl)-6-methyl-2-oxo-pyridine-3-carboxamide (**6**).*

Compound **6** was prepared using 4-methoxyphenylboronic acid and it was purified by flash column chromatography on silica gel (7:3 *n*-hexane/ethyl acetate). **6**: Yield 56%. ^{1}H NMR ($CDCl_3$, 400 MHz) δ: 13.15 (bs, 1H, OH), 9.67 (bd, 1H, *J* = 7.5 Hz, NH), 8.54 (s, 1H, H_4-Py), 7.20 (m, 2H, Ar-*H*), 6.96 (m, 2H, Ar-*H*), 4.25 (m, 1H, CHN), 3.82 (s, 3H, *C*H$_3$O), 2.44 (s, 3H, C*H*$_3$-Py), 1.79 (m, 12H, 6×C*H*$_2$).

*4.1.5.3. N-Cycloheptyl-1,2-dihydro-5-(4-fluorophenyl)-6-methyl-2-oxo-pyridine-3-carboxamide (**7**).*

Compound **7** was prepared using 4-fluorophenyl boronic acid and it was purified by flash column chromatography on silica gel ((1:1 petroleum ether/ethyl acetate). **7**: Yield 57 %. ^{1}H NMR ($CDCl_3$, 400 MHz) δ: 13.30 (bs, 1H, OH), 9.62 (bd, 1H, *J* = 7.8 Hz, NH), 7.23 (m, 3H, H_4-Py, Ar-*H*), 7.09

(m, 2H, Ar-*H*), 4.20 (m, 1H, CHN), 2.39 (s, 3H, C*H*$_3$-Py), 2.04 (m, 2H, C*H*$_2$), 1.53 (m, 10H, 5×C*H*$_2$). ^{13}C NMR ($CDCl_3$, 100 MHz) δ: (ppm) 163.93 (C=O), 162.49 (d, $J_{C\text{-}F}$ = 246 Hz, Ar-*C*F), 162.44 (C=O), 147.00 (*C*$_6$-Py), 146.17 (*C*$_4$-Py), 132.76 (d, $J_{C\text{-}F}$ = 3 Hz, Ar-*C*), 131.08 (d, $J_{C\text{-}F}$ = 8 Hz, 2×Ar-*C*H), 121.14 (*C*$_5$-Py), 118.74 (*C*$_3$-Py), 115.86 (d, $J_{C\text{-}F}$ = 21 Hz, 2×Ar-*C*H), 49.99 (CH-NH), 34.96 (2×CH_2CHNH), 28.34 (2×CH_2), 24.07 (2×CH_2), 17.87 (CH_3-Py).

*4.1.6. Tert-butyl 4-(2-hydroxy-6-methylnicotinamido)piperidine-1-carboxylate (**8**).*

Compound **8** was prepared from compound 1,2-dihydro-6-methyl-2-oxo-pyridine-3-carboxilyc acid as described for compound **1** using *tert*-butyl-4-aminopiperidine-1-carboxylate and it was purified by flash chromatography on silica gel (ethyl acetate and 1% NEt_3). **8**: Yield 64%. ^{1}H NMR ($CDCl_3$, 400 MHz) δ: 12.67 (bs, 1H, OH), 9.62 (bd, 1H, *J* = 7.6 Hz, NH), 8.50 (d, 1H, *J* = 7.4 Hz, H$_4$-Py), 6.34 (d, 1H, *J* = 7.4 Hz, H$_5$-Py), 4.13 (m, 1H, CHN), 3.94, 3.05 (2m, each 2H, 2×C*H*$_2$CHNH), 2.42 (s, 3H, C*H*$_3$-Py), 1.98, 1.65 (2m, each 2H, 2×C*H*$_2$CHN), 1.46 (s, 9H, (C*H*$_3$)$_3$C).

*4.1.7. 1,2-Dihydro-5-bromo-1-(4-fluorobenzyl)-6-methyl-2-oxo-pyridine-3-carboxylic acid (**10**).*

Cesium fluoride (3.20 g, 21.03 mmol) was added to a solution of 1,2-dihydro-6-methyl-2-oxo-pyridine-3-carboxilyc acid (1.07 g, 7.01 mmol) in anhydrous DMF (15.0 mL). After 1 h, *p*-fluorobenzyl chloride (2.5 mL, 21.03 mmol) was added, and the resulting mixture was left under stirring at 65 °C for 20 h. After that, the reaction mixture was concentrated under reduced pressure and the residue was refluxed for 4 h in 10% aqueous NaOH (35.0 mL). After cooling to room temperature, the reaction was acidified with 1N aqueous HCl and the precipitated was collected by filtration to afford compound **10** as a yellow solid (1.02 g, 3.92 mmol), which was used in the

next step without further purification. **10**: Yield 56 %. ^{1}H NMR ($CDCl_3$, 400 MHz) δ: 8.43 (d, 1H, J = 7.6 Hz, H_4-Py), 7.16 (m, 2H, Ar-*H*), 7.04 (m, 2H, Ar-*H*), 6.45 (d, 1H, J = 7.6 Hz, H_5-Py), 5.41 (s, 2H, PhCH_2N), 2.46 (s, 3H, CH_3-Py).

*4.1.8. 1-(4-Fluorobenzyl)-N-(((3aS,4R,6R,7R,7aR)-7-hydroxy-6-methoxy-2,2-dimethyltetrahydro-4H-[1,3]dioxolo[4,5-c]pyran-4-yl)methyl)-6-methyl-2-oxo-1,2-dihydropyridine-3-carboxamide (**13**).*

Compound **13** was prepared from compound **10** as described for compound **1** using the monosaccharide derivative **11**[19] and it was purified by flash chromatography on silica gel (9:1 $CHCl_3$/MeOH). **13**: Yield 93%. ^{1}H NMR (CD_3CN, 250.13 MHz) δ: 10.1 (bt, 1H, NH), 8.35 (d, 1H, J = 7.5 Hz, H_4-Py), 7.19 (m, 2H, Ar-*H*) 7.08 (m, 2H, Ar-*H*), 6.40 (d, 1H, J = 7.5 Hz, H_5-Py), 5.36 (s, 2H, PhCH_2N), 4.17 (dd, 1H, $J_{4,5}$ = 2.2 Hz, $J_{3,4}$ = 5.6 Hz, H-4), 4.06 (d, 1H, $J_{1,2}$ = 8.2 Hz, H-1), 3.98 (dd, 1H, $J_{2,3}$= 7.2 Hz, $J_{3,4}$ = 5.6 Hz, H-3), 3.93 (ddd, 1H, $J_{5,6b}$ = 4.6 Hz, $J_{5,6a}$ = 8.7 Hz, $J_{4,5}$ = 2.2 Hz, H-5), 3.77 (ddd, 1H, $J_{6a,6b}$ = 13.6 Hz, $J_{6b,NH}$= 4.7 Hz, $J_{5,6b}$ = 4.6 Hz, H-6b), 3.50 (ddd, 1H, $J_{6a,6b}$ = 13.6 Hz, $J_{5,6a}$ = 8.7 Hz, $J_{6a,NH}$= 6.8 Hz, H-6a), 3.43 (s, 3H, OCH_3), 3.42 (d, 1H, $J_{2,OH}$ = 3.5 Hz, OH), 3.33 (ddd, 1H, $J_{1,2}$ = 8.2 Hz, $J_{2,3}$= 7.2 Hz, $J_{2,OH}$ = 3.5 Hz, H-2), 2.40 (s, 3H, CH_3-Py), 1.46, 1.31 (2s, each 3H, CMe_2); ^{13}C NMR (CD_3CN, 62.9 MHz) δ: 164.99, 163.90 (2×C=O), 163.0 (d, $J_{C\text{-}F}$ = 241.6 Hz, Ar-*CF*), 153.18 (C_6-Py), 143.65 (C_4-Py), 133.31 (d, $J_{C\text{-}F}$ = 3.1 Hz, Ar-*C*), 129.42 (d, $J_{C\text{-}F}$ = 8.3 Hz, 2×Ar-*C*H), 118.78, (C_3-Py), 116.32, (d, $J_{C\text{-}F}$ = 22.0 Hz, 2×Ar-*C*H), 110.37 (*C*Me$_2$), 108.55 (C_5-Py), 104.33 (C-1), 80.32 (C-3), 75.11 (C-4), 74.18 (C-2), 71.97 (C-5), 56.87 (OMe), 47.91 (Ph*C*H$_2$N), 40.64 (C-6), 28.36, 26.52 (CMe_2), 21.38 (*C*H$_3$-Py).

*4.1.9. (2R,3S,4R,5R,6R)-5-Acetamido-2-(acetoxymethyl)-6-(1-(4-fluorobenzyl)-6-methyl-2-oxo-1,2-dihydropyridine-3-carboxamido)tetrahydro-2H-pyran-3,4-diyl diacetate (**14**).*

Compound **14** was prepared from compound **10** as described for compound **1** using the monosaccharide **12**[20] and it was purified by flash chromatography on silica gel (9.8:0.2 $CHCl_3$/MeOH). **14**: Yield: 50 %. ^{1}H NMR (CD_3CN, 250.13 MHz) δ: 10.3 (d, 1H, $J_{1,NH}$ = 9.3 Hz, NH), 8.37 (d, 1H, J = 7.6 Hz, H_4-Py), 7.33-7.06 (m, 4H, Ar-*H*), 6.54 (d, 1H, $J_{2,NH}$= 9.5 Hz, NH), 6.43 (d, 1H, J = 7.6 Hz, H_5-Py), 5.46, 5.37 (AB system, 2H, $J_{A,B}$ = 15.7 Hz, PhCH_2N), 5.25 (dd, 1H, $J_{2,3}$= 10.1 Hz, $J_{3,4}$= 9.6 Hz, H-3), 5.02 (dd, 1H, $J_{4,5}$= 10.3 Hz, $J_{3,4}$= 9.6 Hz H-4), 5.49 (dd, 1H, $J_{1,2}$= 9.5 Hz, $J_{1,NH}$ = 9.3 Hz, H-1), 4.14 (m, 1H, H-2), 4.19 (dd, 1H, $J_{6a,6b}$ = 12.2 Hz, $J_{5,6b}$= 5.0 Hz, , H-6b), 4.05 (dd, 1H, $J_{6a,6b}$ = 12.2 Hz, $J_{5,6a}$= 2.3 Hz, H-6a), 3.90 (ddd, 1H, $J_{4,5}$= 10.3 Hz, $J_{5,6b}$= 5.0 Hz, $J_{5,6a}$= 2.3 Hz, H-5), 2.40 (s, 3H, CH_3-Py), 2.01, 2.00, 1.97 (3s, each3H, 3×*Me*COO), 1.76 (s, 3H, *Me*CON). ^{13}C NMR (CD_3CN, 62.9 MHz) δ: 171.29, 171.14, 170.93, 170.54 (4×C=O), 165.49, 163.81 (2×C=O), 162.9 (d, $J_{C\text{-}F}$ = 236.4 Hz, Ar-*C*F), 154.39 (C_6-Py), 144.63 (C_4-Py), 133.05 (d, $J_{C\text{-}F}$ = 3.6 Hz, Ar-*C*), 129.32 (d, $J_{C\text{-}F}$ = 8.2 Hz, 2×Ar-*C*H), 117.67 (C_3-Py), 116.42 (d, $J_{C\text{-}F}$ = 21.9 Hz, 2×Ar-*C*H), 108.84 (C_5-Py), 79.26 (C-1), 74.11 (C-5), 73.96 (C-3), 69.60 (C-4), 63.09 (C-6), 53.56 (C-2), 47.92 (Ph*C*H_2N), 22.92 (*Me*CON), 21.43 (*C*H_3-Py), 20.86 (3×*Me*COO).

*4.1.10. (2R,3S,4R,5R,6R)-5-Acetamido-2-(acetoxymethyl)-6-(5-bromo-1-(4-fluorobenzyl)-6-methyl-2-oxo-1,2-dihydropyridine-3-carboxamido)tetrahydro-2H-pyran-3,4-diyl diacetate (**15**).*

Compound **15** was prepared from compound **14** as described for compound **2** and it was purified by flash chromatography on silica gel (ethyl acetate). **15**: 32 %. ^{1}H NMR (CD_3CN, 250.13 MHz) δ: 10.2 (d, 1H, $J_{1,NH}$= 9.0 Hz, NH), 8.49 (s, 1H, H_4-Py), 7.19 (m, 2H, Ar-*H*) 7.08 (m, 2H, Ar-*H*), 6.60 (d, 1H, $J_{2,NH}$ = 9.6 Hz, NH), 5.49 (s, 2H, PhCH_2N), 5.40 (dd, 1H, $J_{1,2}$ = 9.5 Hz, $J_{1,NH}$= 9.0 Hz,

H-1), 5.24 (dd, 1H, $J_{2,3}$ = 10.4 Hz, $J_{3,4}$ = 9.4 Hz, H-3), 5.00 (dd, 1H, $J_{4,5}$ = 10.0 Hz, $J_{3,4}$ = 9.4 Hz, H-4), 4.22 (dd, 1H, $J_{6a,6b}$ = 12.6 Hz, $J_{5,6b}$ = 4.8 Hz, H-6b), 4.14 (m, 1H, H-2), 4.03 (dd, 1H, $J_{6a,6b}$ = 12.6 Hz, $J_{5,6a}$ = 2.6 Hz, H-6a), 3.90 (ddd, 1H, $J_{4,5}$ = 10.0 Hz, $J_{5,6b}$ = 4.8 Hz, $J_{5,6a}$ = 2.6 Hz, H-5), 2.51 (s, 3H, C*H*$_3$-Py), 2.00, 1.98, 1.95 (3s, each 3H, 3×*Me*COO), 1.75 (s, 3H, *Me*CON). ^{13}C NMR (CD_3CN, 62.9 MHz) δ: 171.20, 171.17, 170.58, 170.6 (4×C=O), 164.30, 162.77 (2×C=O), 162.63 (d, $J_{C\text{-}F}$ = 221.4 Hz, Ar-*CF*), 152.49 (*C*$_6$-Py), 147.55 (*C*$_4$-Py), 132.51 (d, $J_{C\text{-}F}$ = 2.2 Hz, Ar-*C*), 129.31 (d, $J_{C\text{-}F}$ = 8.2 Hz, 2×Ar-*C*H), 118.82 (*C*$_3$-Py), 116.41 (d, $J_{C\text{-}F}$ = 21.8 Hz, 2×Ar-*C*H), 101.86 (C$_5$-Py), 79.30 (C-1), 74.14 (C-5), 73.82 (C-3), 69.53 (C-4), 63.04 (C-6), 53.51 (C-2), 49.58 (Ph*C*H$_2$N), 22.90 (*Me*CON), 21.55 (*C*H$_3$-Py), 20.85 (3×*Me*COO).

*4.1.11. General procedure for the synthesis of N_1-substituted **9, B1-B7** and O-substituted* **C1, C2, C6** and **C7** *pyridine-3-carboxamide derivatives*

Cesium carbonate (0.30 mmol) was added to a solution of the suitable 6-methyl-2-oxo-pyridine-3-carboxamide (0.3 mmol) in anhydrous DMF (0.9 mL). After 1 h, *p*-fluorobenzyl chloride (0.90 mmol) was added, and the resulting mixture was left under stirring at 25 °C for 12 h. After cooling to room temperature, the reaction mixture was concentrated under reduced pressure, treated with water, and then extracted with dichloromethane. The organic layer was dried over anhydrous Na_2SO_4, filtered, and evaporated under reduced pressure to give a residue which was purified by flash chromatography.

*4.1.11.1. tert-butyl 4-(1-(4-Fluorobenzyl)-6-methyl-2-oxo-1,2-dihydropyridine-3-carboxamido) piperidine–1–carboxylate (**9**).*

Compound **9** was prepared from compound **1** and it was purified by flash chromatography (3:7 *n*-hexane/ethyl acetate). **9**: Yield 38%. ^{1}H NMR ($CDCl_3$, 400 MHz) δ: 9.75 (bd, 1H, *J* = 8.2 Hz, NH), 8.44 (d, 1H, *J* = 7.6 Hz, H_4-Py), 7.09 (m, 2H), Ar-H, 7.01 (m, 2H, Ar-H), 6.31 (d, 1H, *J* = 7.6 Hz, H_5-Py), 5.35 (s, 2H, PhC*H*$_2$N), 4.13 (m, 1H, C*H*N), 3.94, 2.97 (2m, each 2H, 2×C*H*$_2$CHNH), 2.36 (s, 3H, C*H*$_3$-Py), 1.95, 1.49 (2m, each 2H, 2×C*H*$_2$CHN), 1.46 (s, 9H, (C*H*$_3$)$_3$C).

*4.1.11.2. N-Cycloheptyl-1,2-dihydro-1-(4-fluorobenzyl)-6-methyl-2-oxo-pyridine-3-carboxamide (**B1**) and N-cycloheptyl-2-((4-fluorobenzyl)oxy)-6-methylnicotinamide (**C1**).*

Compound **B1** was prepared from compound **1**. The purification of reaction mixture by flash chromatography on silica gel (7:3 *n*-hexane/ethyl acetate) allowed also to obtain the *O*-substituted pyridine-3-carboxamide derivative **C1**. **B1**: Yield 12%. Mp: 107-109 °C. ^{1}H NMR ($CDCl_3$, 400 MHz) δ: 9.70 (bd, 1H, *J* = 7.2 Hz, NH), 8.45 (d, 1H, *J* = 7.6 Hz, H_4-Py), 7.09 (m, 2H, Ar-H), 7.01 (m, 2H, Ar-H), 6.29 (d, 1H, *J* = 7.6 Hz, H_5-Py), 5.36 (s, 2H, PhC*H*$_2$N), 4.12 (m, 1H, CHN), 2.35 (s, 3H, C*H*$_3$-Py), 1.98 (m, 2H, CH_2) 1.59 (m, 10H, 5×CH_2).^{13}C NMR ($CDCl_3$, 100 MHz) δ: 163.14, 162.74 (2×C=O), 162.21 (d, $J_{C,F}$ = 245 Hz, Ar-*C*F), 150.34 (*C*$_6$-Py), 143.02 (*C*$_4$-Py), 131.19 (d, $J_{C,F}$ = 4 Hz, Ar-*C*), 128.01 (d, $J_{C,F}$ = 8 Hz, 2×Ar-*C*H), 119.04 (*C*$_3$-Py), 115.98 (d, $J_{C,F}$ = 22 Hz, 2×Ar-*C*H), 108.08 (C_5-Py) 50.42 (Ph*C*H_2N), 47.11 (CHN), 34.99 (2×*C*H_2CHN) 28.15 (2×*C*H_2), 24.27 (2×*C*H_2), 21.14 (*C*H_3-Py). HPLC analysis: retention time = 15.68 min; peak area 97.56 % (280 nm). **C1**: Yield 30%. Mp: 191-194 °C. ^{1}H NMR ($CDCl_3$, 400 MHz) δ: 8.39 (d, 1H, *J* = 7.6 Hz, H_4-Py), 7.88 (bd, 1H, *J* = 7.4 Hz, NH), 7.46 (m, 2H, Ar-H), 7.10 (m, 2H, Ar-H), 6.90 (d, 1H, *J* = 7.6 Hz, H_5-Py), 5.44 (s, 2H, PhC*H*$_2$O), 4.12 (m, 1H, CHN), 2.49 (s, 3H, C*H*$_3$-Py), 1.83 (m, 2H, CH_2), 1.40 (m, 10H, 5×CH_2). ^{13}C NMR ($CDCl_3$, 100 MHz) δ: 162.80 (d, $J_{C,F}$ = 246 Hz, Ar-*C*F),

162.62 (C=O), 159.30 (*C*$_2$-Py, *C*$_6$-Py), 141.81 (*C*$_4$-Py), 132.25 (d, $J_{C,F}$= 3 Hz, Ar-*C*), 130.69 (d, $J_{C,F}$= 8 Hz, 2×Ar-*C*H), 128.58 (Ar-*C*), 117.29 (*C*$_3$-Py), 115.58 (d, $J_{C,F}$= 21 Hz, 2×Ar-*C*H), 113.25 (C$_5$-Py), 68.03 (Ph*C*H$_2$O), 49.86 (CHN), 34.62 (2×*C*H$_2$CHN), 28.22 (2×*C*H$_2$), 24.05 (2×*C*H$_2$), 23.62 (*C*H$_3$-Py). HPLC analysis: retention time = 14.23 min; peak area 95.90 % (280 nm).

*4.1.11.3. N-Cycloheptyl-1,2-dihydro-5-bromo-1-(4-fluorobenzyl)-6-methyl-2-oxo-pyridine-3-carboxamide (**B2**) and 5-bromo-N-cycloheptyl-2-((4-fluorobenzyl)oxy)-6-methylnicotinamide (**C2**).*

Compound **B2** was prepared from compound **2**. The purification by flash column chromatography on silica gel (9:1 petroleum ether/ethyl acetate) also enabled us to obtain the *O*-substituted pyridine-3-carboxamide derivative **C2**. **B2**: Yield 22%. Mp: 146-149 °C. ^{1}H NMR (CDCl$_3$, 400 MHz) δ: 9.60 (bd, 1H, *J* = 8.0 Hz, NH), 8.65 (s, 1H, H$_4$-Py), 7.07 (m, 4H, Ar-H), 5.42 (s, 2H, PhC*H*$_2$N), 4.13 (m, 1H, CHN), 2.52 (s, 3H, C*H*$_3$-Py), 2.00 (m, 2H, CH$_2$), 1.59 (m, 10H, 5×CH$_2$). ^{13}C NMR (CDCl$_3$, 100 MHz) δ: 162.38 (d, $J_{C,F}$ = 246 Hz, Ar-*C*F), 162.10, 161.47 (2×C=O), 148.42 (*C*$_6$-Py) 146.56 (*C*$_4$-Py), 130.75 (d, $J_{C,F}$ = 3 Hz, Ar-*C*), 128.07 (d, $J_{C,F}$ = 8 Hz, 2×Ar-*C*H), 120.11 (Ar-*C, C*$_3$-Py), 116.21 (d, $J_{C,F}$ = 22 Hz, 2×Ar-*C*H), 101.92 (C$_5$-Py), 50.64 (Ph*C*H$_2$N), 48.76 (CHN), 34.96 (2×*C*H$_2$CHN), 28.19 (2×*C*H$_2$), 24.25 (2×*C*H$_2$), 20.89 (*C*H$_3$-Py). HPLC analysis: retention time = 14.37 min; peak area 95.82 % (280 nm). HRMS-ESI: m/z calcd for C$_{21}$H$_{24}$BrFN$_2$O$_2$ [M+H]$^+$, 435.10780; found 435.10797. **C2**: Yield 50%. Mp 86-89 °C. ^{1}H NMR (CDCl$_3$, 400 MHz) δ: 8.56 (s, 1H, H$_4$-Py), 7.80 (bd, 1H, NH), 7.45 (m, 2H, Ar-H), 7.11 (m, 2H, Ar-H), 5.41 (s, 2H, PhC*H*$_2$O), 4.12 (m, 1H, CHN), 2.60 (s, 3H, C*H*$_3$-Py), 1.82 (m, 2H, CH$_2$), 1.45 (m, 10H, 5×CH$_2$). ^{13}C NMR (CDCl$_3$, 100 MHz) δ: 163.06 (d, $J_{C,F}$ = 247 Hz, Ar-*C*F), 161.42 (C=O), 158.04, 157.66 (*C*$_2$-Py, *C*$_6$-Py),14.88 (*C*$_4$-Py), 132.00 (d, $J_{C,F}$ = 3 Hz, Ar-*C*), 130.90 (d, $J_{C,F}$ = 9 Hz,

2×Ar-*C*H), 115.86 (d, $J_{C,F}$ = 22 Hz, 2×Ar-*C*H), 115.54 (*C*$_3$-Py), 113.60 (*C*$_5$-Py), 68.71 (Ph*C*H$_2$O), 50.18 (CHN), 34.75 (2×*C*H$_2$), 29.83 (2×*C*H$_2$), 28.36 (2×*C*H$_2$), 23.76 (*C*H$_3$-Py). HPLC analysis: retention time = 20.30 min; peak area 95.96 % (280 nm).

*4.1.11.4. N-Cycloheptyl-1,2-dihydro-5-chloro-1-(4-fluorobenzyl)-6-methyl-2-oxo-pyridine-3-carboxamide (**B3**).*

Compound **B3** was prepared from compound **3** and it was purified by flash chromatography on silica gel (9:1 petroleum ether/ethyl acetate). **B3**: Yield 22%. Mp: 97-99 °C. ^{1}H NMR (CDCl$_3$, 400 MHz) δ: 9.63 (bd, 1H, *J* = 8.0 Hz, NH), 8.54 (s, 1H, H$_4$-Py), 7.08 (m, 4H, Ar-H), 5.42 (s, 2H, PhC*H*$_2$N), 4.18 (m, 1H, CHN), 2.48 (s, 3H, C*H*$_3$-Py), 2.00 (m, 2H, CH$_2$), 1.62 (m, 10H, 5×CH$_2$). ^{13}C NMR (CDCl$_3$, 100 MHz) δ: 162.64 (d, $J_{C,F}$ = 210 Hz, Ar-*C*F), 161.93, 161.59 (2×C=O), 147.14 (*C*$_6$-Py), 144.03 (*C*$_4$-Py), 130.81 (d, $J_{C,F}$= 3 Hz, Ar-*C*), 128.14 (d, $J_{C,F}$= 8 Hz, 2×Ar-*C*H), 120.03 (Ar-*C,* *C*$_3$-Py), 116.27 (d, $J_{C,F}$= 22 Hz, 2×Ar-*C*H), 114.08 (C$_5$-Py), 50.71 (Ph*C*H$_2$N), 48.53 (CHN), 35.03 (2×*C*H$_2$CHN),28.25 (2×*C*H$_2$), 24.33 (2×*C*H$_2$), 18.08 (*C*H$_3$-Py). HPLC analysis: retention time = 14.03 min; peak area 97.44 % (280 nm).

*4.1.11.5. N-Cycloheptyl-1,2-dihydro-5-fluoro-1-(4-fluorobenzyl)-6-methyl-2-oxo-pyridine-3-carboxamide (**B4**).*

Compound **B4** was prepared from compound **4** and it was purified by flash chromatography on silica gel (9:1 petroleum ether/ethyl acetate). **B4**: Yield 10%. ^{1}H NMR (CDCl$_3$, 400 MHz) δ: 9.73 (bd, 1H, *J* = 7.2 Hz, NH), 8.45 (d, 1H, $J_{H,F}$ = 9.2 Hz, H$_4$-Py), 7.12 (m, 2H, Ar-H), 7.03 (m, 2H Ar-H), 5.35 (s, 2H, PhC*H*$_2$N), 4.13 (m, 1H, CHN), 2.33 (d, 3H, $J_{H,F}$= 3.2 Hz, C*H*$_3$-Py), 1.99 (m, 2H, CH$_2$), 1.60 (m, 10H, 5×CH$_2$). ^{13}C NMR (CDCl$_3$, 100 MHz) δ: 162.39 (d, $J_{C,F}$ = 248 Hz, Ar-*C*F),

161.71, 161.68 (2×C=O), 145.83 (d, $J_{C,F}$ = 227 Hz, C_5-Py), 136.69 (d, $J_{C,F}$= 28 Hz, C_4-Py), 133.17 (d, $J_{C,F}$ = 27 Hz, C_6-Py), 130.83 (d, $J_{C,F}$= 3 Hz, Ar-*C*), 128.21 (d, $J_{C,F}$= 8 Hz, 2×Ar-*C*H), 119.46 (d, $J_{C,F}$= 5 Hz, C_3-Py), 116.22 (d, $J_{C,F}$ = 22 Hz, 2×Ar-*C*H), 50.73 (Ph*C*H_2N), 47.71 (CHN), 35.01 (2×*C*H_2CHN), 28.22 (2×*C*H_2), 24.32 (2×*C*H_2), 13.00 (*C*H_3-Py). HPLC analysis: retention time = 11.95 min; peak area 97.59 % (280 nm).

*4.1.11.6. N-Cycloheptyl-1,2-dihydro-1-(4-fluorobenzyl)-6-methyl-2-oxo-5-phenyl-pyridine-3-carboxamide (**B5**).*

Compound **B5** was prepared from compound **5** and it was purified by flash chromatography on silica gel (7:3 *n*-hexane/ethyl acetate) **B5**: Yield 25%. Mp: >190 °C dec. ^{1}H NMR ($CDCl_3$, 400 MHz) δ: 9.79 (bd, 1H, *J* = 8.0 Hz, NH), 8.50 (s, 1H, H_4-Py), 7.38 (m, 3H, Ar-H), 7.21 (m, 2H, Ar-H), 7.13 (m, 2H, Ar-H), 7.04 (m, 2H, Ar-H), 5.46 (s, 2H, PhC*H*$_2$N), 4.15 (m, 1H, CHN), 2.30 (s, 3H, C*H*$_3$-Py), 1.98 (m, 2H, CH_2), 1.57 (m, 10H, 5×CH_2). ^{13}C NMR ($CDCl_3$, 100 MHz) δ: 162.74, 162.61 (2×C=O), 162.32 (d, $J_{C.F}$ = 245 Hz, Ar-*C*F), 147.46 (C_6-Py), 145.21 (C_4-Py), 138.14 (Ar-*C*), 131.36 (d, $J_{C.F}$= 4 Hz, Ar-*C*), 129.74 (Ar-*C*H), 128.76(Ar-*C*H), 128.08 (d, $J_{C.F}$= 8 Hz, 2×Ar-*C*H), 127.82 (Ar-*C*H), 122.07 (C_3-Py), 118.64 (C_5-Py)116.13 (d, $J_{C.F}$= 21 Hz, 2×Ar-*C*H), 50.54 (Ph*C*H_2N), 47.89 (CHN), 35.08 (2×*C*H_2CHN), 28.27 (2×*C*H_2), 24.33 (2×*C*H_2), 18.70 (*C*H_3-Py). HPLC analysis: retention time = 15.73 min; peak area 97.04 % (280 nm).

*4.1.11.7. N-Cycloheptyl-1,2-dihydro-5-(4-methoxyphenyl-1-(4-fluorobenzyl))-6-methyl-2-oxo-pyridine-3-carboxamide (**B6**) and N-cycloheptyl-2-((4-fluorobenzyl)oxy)-5-(4-methoxyphenyl)-6-methylnicotinamide (**C6**).*

Compound **B6** was prepared from compound **6**. The purification by flash chromatography on silica gel (8:2 petroleum ether/ethyl acetate) allowed also to obtain the *O*-substituted pyridine-3-carboxamide derivative **C6**. **B6**: Yield 25%. Mp: 163-166 °C. ^{1}H NMR ($CDCl_3$, 400 MHz) δ: 9.79 (bd, 1H, *J* = 7.6 Hz, NH), 8.50 (s, 1H, H_4-Py), 7.14 (m, 4H, Ar-H), 7.04 (m, 2H, Ar-H), 6.92 (m, 2H, Ar-H), 5.46 (s, 2H, PhC*H*$_2$N), 4.14 (m, 1H, CHN), 3.83 (s, 3H, C*H*$_3$O), 2.30 (s, 3H, C*H*$_3$-Py), 2.00 (m, 2H, CH_2), 1.60 (m, 10H, 5×CH_2). ^{13}C NMR ($CDCl_3$, 100 MHz) δ: 162.81, 162.57 (2×C=O), 162.30 (d, $J_{C,F}$= 245 Hz, Ar-*C*F), 159.21 (Ar-*C*O), 147.48 (C_6-Py)145.39 (C_4-Py), 131.41 (d, $J_{C,F}$= 3 Hz, Ar-*C*), 130.84 (2×Ar-*C*H), 130.40 (Ar-*C*), 128.06 (d, $J_{C,F}$= 8 Hz, 2×Ar-*C*H), 121.74 (C_3-Py), 118.48 (C_5-Py), 116.11 (d, $J_{C,F}$= 22 Hz, 2×Ar-*C*H), 114.14 (2×Ar-*C*H), 55.43 (*C*H_3O), 50.53 (Ph*C*H_2N), 47.90 (CHN), 35.07 (2×*C*H_2CHN), 28.26 (2×*C*H_2), 24.33 (2×*C*H_2), 18.69 (*C*H_3-Py). HPLC analysis: retention time = 15.03 min; peak area 99.50 % (280 nm). **C6**: Yield 38%. ^{1}H NMR ($CDCl_3$, 400 MHz) δ: 8.34 (s, 1H, H_4-Py), 7.91 (bd, 1H, NH), 7.48 (m, 2H, Ar-H), 7.23 (m, 2H, Ar-H), 7.11 (m, 2H, Ar-H), 6.93 (m, 2H, Ar-H), 5.49 (s, 2H, PhC*H*$_2$O), 4.15 (m, 1H, CHN), 3.85 (s, 3H, C*H*$_3$O), 2.46 (s, 3H, C*H*$_3$-Py), 1.85 (m, 2H, CH_2), 1.52 (m, 10H, 5×CH_2). ^{13}C NMR ($CDCl_3$, 100 MHz) δ: 162.87 (d, $J_{C,F}$ = 246 Hz, Ar-*C*F), 162.66 (C=O), 158.94, 157.94156.37 (Ar-*C*O, C_6-Py, C_2-Py), 142.92 (C_4-Py), 132.43 (d, $J_{C,F}$= 4 Hz, Ar-*C*), 131.30 (Ar-*C*), 131.14 (2×Ar-*C*H), 130.76 (d, $J_{C,F}$= 8 Hz, 2×Ar-*C*H), 130.36 (C_3-Py),115.66 (d, $J_{C,F}$= 22 Hz, 2×Ar-*C*H), 113.83 (2×Ar-*C*H),113.48 (C_5-Py), 68.19 (Ph*C*H_2O), 55.31 (*C*H_3O), 49.94 (CHN), 34.71 (2×*C*H_2CHN), 28.29 (2×*C*H_2), 23.70 (2×*C*H_2), 23.10 (*C*H_3-Py). HPLC analysis: retention time = 17.52 min; peak area 98.21 % (280 nm).

*4.1.11.8. N-Cycloheptyl-5-(4-fluorophenyl)-1-(4-fluorobenzyl)-6-methyl-2-oxo-1,2-dihydropyridin-3-carboxamide (**B7**) and N-cycloheptyl-5-(4-fluorophenyl)-6-methyl-2-((4-fluorobenzyl)oxi)-pyiridin-3-carboxamide (**C7**).*

Compound **B7** was prepared from compound **7**. Purification by flash chromatography on silica gel (3:7 petroleum ether/ethyl acetate) allowed also to obtain the *O*-substituted pyridine-3-carboxamide derivative **C7. B7**: Yield 50 %. Mp: 178-179 °C. ^{1}H NMR ($CDCl_3$, 400 MHz) δ: 9.75 (bd, 1H, J = 8.0 Hz, NH), 8.47 (s, 1H, H_4-Py), 7.12 (m, 8H, Ar-H), 5.46 (s, 2H, PhCH_2N), 4.15 (m, 1H, CHN), 2.28 (s, 3H, CH_3-Py), 2.01 (m, 2H, CH_2), 1.62 (m, 10H, 5×CH_2). ^{13}C NMR ($CDCl_3$, 100 MHz) δ: 162.47, 162.43 (2×C=O), 162.26 (d, $J_{C,F}$= 246 Hz, Ar-*C*F), 162.20 (d, $J_{C,F}$= 245 Hz, Ar-*C*F), 147.43 (C_6-Py),144.92 (C_4-Py), 133.96 (d, $J_{C,F}$ = 3 Hz, Ar-*C*), 131.29 (d, $J_{C,F}$ = 8 Hz, 2×Ar-*C*H), 131.14 (d, $J_{C,F}$ = 3 Hz, Ar-*C*), 127.96 (d, $J_{C,F}$ = 8 Hz, 2×Ar-*C*H), 120.81 (C_3-Py), 118.57 (C_5-Py), 116.01 (d, $J_{C,F}$ = 22 Hz, 2×Ar-*C*H), 115.65 (d, $J_{C,F}$ = 21 Hz, 2×Ar-*C*H), 50.41 (Ph*C*H_2N), 47.77 (CHN), 34.92 (2×*C*H_2CHN), 28.11 (2×*C*H_2), 24.18 (2×*C*H_2), 18.53 (*C*H_3-Py). HPLC analysis: retention time = 15.70 min; peak area 97.87 % (280 nm). **C7**: Yield 18 % Mp: 137-139 °C. ^{1}H NMR ($CDCl_3$, 400 MHz) δ: 8.34 (s, 1H, H_4-Py), 7.91 (bd, 1H, J = 4.0 Hz, NH), 7.51 (m, 2H, Ar-H), 7.27 (m, 2H, Ar-H), 7.12 (m, 4H, Ar-H), 5.49 (s, 2H, PhCH_2O), 4.15 (m, 1H, CHN), 2.45 (s, 3H, CH_3-Py), 1.84 (m, 2H, CH_2), 1.48 (m, 10H, 5×CH_2). ^{13}C NMR ($CDCl_3$, 100 MHz) δ: (ppm) 162.83 (d, $J_{C,F}$= 246 Hz, Ar-*C*F), 162.40 (C=O), 162.16 (d, $J_{C,F}$= 246 Hz, Ar-*C*F), 158.14, 156.23 (C_2-Py, C_6-Py), 142.88 (C_4-Py), 134.89 (d, $J_{C,F}$= 4 Hz, Ar-*C*), 132.25 (d, $J_{C,F}$= 3 Hz, Ar-*C*), 130.81 (d, $J_{C,F}$= 8 Hz, 2×Ar-*C*H), 130.70 (d, $J_{C,F}$= 8 Hz, 2×Ar-*C*H), 130.40 (C_3-Py),115.64 (d, $J_{C,F}$ = 21 Hz, 2×Ar-*C*H), 115.30 (d, $J_{C,F}$ = 22 Hz, 2×Ar-*C*H), 113.55 (C_5-Py),68.21 (Ph*C*H_2O), 49.90 (CHN), 34.64 (2×*C*H_2CHN), 28.22 (2×*C*H_2), 23.63 (2×*C*H_2), 22.94 (*C*H_3-Py). HPLC analysis: retention time = 20.90 min; peak area 97.56 % (280 nm).

*4.1.12. 5-Bromo-1-(4-fluorobenzyl)-6-methyl-2-oxo-N-(piperidin-4-yl)-1,2-dihydropyridine-3-carboxamide (**B8**).*

Compound **B8** was prepared from compound **9** as described for compound **2**. The mixture was filtered to recover the compound precipitated as solid from the organic layer. Once collected, the yellow solid was treated with a solution of NaOH 10% and the with H_2O allowing the isolation of the pure final compound **B8** as a white solid. **B8**: Yield 58 % Mp: 193-196 °C. ^{1}H NMR ($CDCl_3$, 400 MHz) δ: 9.60 (bd, 1H, J = 8.0 Hz, NH), 8.65 (s, 1H, H_4-Py), 7.06 (m, 4H, Ar-H), 5.42 (s, 2H, PhCH_2N), 4.05 (m, 1H, CHN), 3.07, 2.73 (2m, each 2H, 2×CH_2NH), 2.52 (s, 3H, CH_3-Py), 1.99, 1.47 (2m, each 2H, 2×CH_2CHN). ^{13}C NMR ($CDCl_3$, 100 MHz) δ: 162.47 (d, $J_{C,F}$ = 246 Hz, Ar-*C*F), 162.16, 161.95 (2×C=O), 148.69 (C_6-Py),146.75 (C_4-Py), 130.73 (d, $J_{C,F}$= 3 Hz, Ar-*C*), 128.12 (d, $J_{C,F}$= 8 Hz, 2×Ar-*C*H), 119.95 (C_3-Py),116.30 (d, $J_{C,F}$= 22 Hz, 2×Ar-*C*H), 101.99 (C_5-Py), 48.85 (Ph*C*H_2N), 47.12 (CHN), 45.43 (CH_2NH), 33.47 (CH_2CHN), 20.97 (*C*H_3-Py). HPLC analysis: retention time = 21.13 min; peak area 99.24 % (280 nm).

*4.1.13. 5-Bromo-1-(4-fluorobenzyl)-6-methyl-2-oxo-N-(((2R,3R,4S,5R,6R)-3,4,5-trihydroxy-6-methoxy tetrahydro-2H-pyran-2-yl)methyl)-1,2-dihydropyridine-3-carboxamide (**B9**).*

Compound **B9** was prepared from compound **13** as described for compound **2** and it was purified by flash chromatography on silica gel (9.5:0.5 ethyl acetate/methanol). **B9**: Yield 55 %. Mp: 206-209 °C. ^{1}H NMR (8:2 CD_3OD-CD_3CN, 250.13 MHz) δ: 8.53 (s, 1H, H_4-Py), 7.22 (m, 2H, Ar-*H*), 7.09 (m, 2H, Ar-*H*), 5.50 (s, 2H, Ph*C*H_2N), 4.16 (d, 1H, $J_{1,2}$ = 7.6 Hz, H-1), 3.82-3.73 (m, 2H, H-4, H-6b), 3.68-3.51 (m, 2H, H-3, H-6a), 3.51 (s, 3H, OCH_3), 3.50-3.46 (m, 2H, H-2, H-5), 2.60 (s, 3H, CH_3-Py). ^{13}C NMR (8:2 CD_3OD-CD_3CN, 62.9 MHz) δ: 165.12, 163.08 (2×C=O),

163.1 (d, $J_{C\text{-}F}$ = 247.6 Hz, Ar-*C*F), 152.08 (C_6-Py), 147.12 (C_4-Py), 132.80 (d, $J_{C\text{-}F}$ = 2.9 Hz, Ar-*C*), 129.56 (d, $J_{C\text{-}F}$ = 8.1 Hz, 2×Ar-*C*H), 119.54 (C_3-Py), 116.61 (d, $J_{C\text{-}F}$ = 21.8 Hz, 2×Ar-*C*H), 105.68 (C-1), 101.99 (C_5-Py), 74.60 (C-5), 74.13 (C-3), 72.26 (C-2), 70.34 (C-4), 57.21 (OMe), 49.68 (Ph*C*H_2N), 40.86 (C-6), 21.33 (*C*H_3-Py). HPLC analysis: retention time = 16.13 min; peak area 98.49 % (280 nm).

*4.1.14. N-((2R,3R,4R,5S,6R)-3-Acetamido-4,5-dihydroxy-6-(hydroxymethyl)tetrahydro-2H-pyran-2-yl)-5-bromo-1-(4-fluorobenzyl)-6-methyl-2-oxo-1,2-dihydropyridine-3-carboxamide (**B10**).*

A solution of compound **15** (23.0 mg, 0.034 mmol) in MeOH (0.34 mL) was treated with 7N NH_3/ MeOH (0.34 mL), and the solution was stirred at room temperature for 24 h. Then, the solution was co-evaporated with toluene (4 X 10 mL) under reduced pressure. The trituration of the crude product with Et_2O afforded **B10** as a yellow solid (17.0 mg, 0.031 mmol). **B10**: Yield: 92 %. Mp 141-144 °C. ^{1}H NMR (9:1 CD_3OD-D_2O, 250.13 MHz) δ: 8.52 (s, 1H, H_4-Py), 7.23-7.05 (m, 4H, Ar-*H*), 5.58,5.43 (AB system, 2H, $J_{A,B}$ = 13.0 Hz, Ph*C*H_2N), 5.17 (d, 1H, $J_{1,2}$= 9.6 Hz, H-1), 3.90 (m, 2H, H-2, H-6b), 3.72 (dd, 1H, $J_{6a,6b}$= 12.4 Hz, $J_{5,6a}$= 2.3 Hz, H-6a), 3.51-3.31 (m, 3H, H-3, H-4, H-5), 2.58 (s, 3H, C*H*$_3$-Py), 1.91 (s, 3H, *Me*CON). ^{13}C NMR (9:1 CD_3OD-D_2O, 62.9 MHz) δ: 174.27 (C=O), 166.01, 162.97 (2×C=O), 163.54 (d, $J_{C\text{-}F}$ = 248 Hz, Ar-*C*F), 153.29 (C_6-Py), 147.99 (C_4-Py), 132.54 (Ar-C), 129.64 (d, $J_{C\text{-}F}$ = 8.1 Hz, 2×Ar-CH), 118.63 (C_3-Py), 116.74 (d, $J_{C\text{-}F}$ = 22 Hz, 2×Ar-*C*H), 102.27 (C_5-Py), 80.20 (C-1), 79.57 (C-5), 75.86 (C-3), 71.58 (C-4), 62.46 (C-6), 55.89 (C-2), 49.78 (Ph*C*H_2N), 22.79 (*Me*CON), 21.43 (*C*H_3-Py). HPLC analysis: retention time = 5.80 min; peak area 99.03 % (280 nm).

4.2. Biological assays

4.2.1. CB1R and CB2R binding assays.

Receptor binding experiments were performed with membrane preparations as previously reported [26]. Briefly, clean membranes expressing hCB1 or hCB2 were re-suspended in binding buffer (50 mM Tris-HCl, 2.5 mM EDTA, 5 mM $MgCl_2$, 0.5% fatty acid-free bovine serum albumin (BSA), pH 7.4) and incubated with vehicle or compounds and 0.5 nM of [^{3}H]CP55,940 for 90 min at 30 °C. Non-specific binding was determined in the presence of 10 μM of WIN55,512. After incubation, membranes were filtered through a pre-soaked 96-well microplate bonded with GF/B filters under vacuum and washed twelve times with 150 μL of ice-cold binding buffer. The radioactivity was measured, and the results expressed as [^{3}H]CP55,940 binding.

4.2.2. [^{35}S]GTPγS assays for functional activity at CB1R and CB2R.

Assays were performed as previously described [70]. Briefly, hCB1- and hCB2-expressing membranes (10 μg) were diluted in binding buffer (50 mM Tris-HCl, 3 mM $MgCl_2$, 0.2 mM EDTA, and 100 mM NaCl at pH 7.4 plus 0.5% fatty acid-free BSA) in the presence of 10 μM of GDP and 0.1 nM of [^{35}S]GTPγS. The mixture was kept on ice until the binding reaction was started by adding the vehicle or compounds at different concentrations. In case of competition experiments, membranes were pre-incubated for 30 min with the antagonist. Non-specific binding was measured in the presence of 10 μM of GTPγS. The tubes were incubated at 30 °C for 90 min. The reaction was stopped by rapid filtration through a 96- well microplate bonded with GF/B filters previously pre-soaked with washing buffer (50mM of Tris-HCl pH 7.4 plus 0.1% fatty acid-free BSA). The filters were washed six times with 180 μL of washing buffer under vacuum. The radioactivity was measured, and the results were expressed as [^{35}S]GTPγS binding.

4.2.3. FAAH and MAGL assays.

FAAH and MAGL assays were performed in living U937 cells as previously described [70]. Cells were diluted in culture medium to a final density of 4×10^6/mL and 250 µL (10^6 cells) were used for each condition. Compounds were added at the screening concentration of 10 µM and incubated for 15 min at 37 °C under shacking. For hit compounds (defined as enzymatic inhibition >50% at 10 µM), complete concentration-dependent experiments were performed to calculate IC_{50} values. After pre-incubation, cells were added with 1 µM of AEA containing 1 nM of [ethanolamine-1-3H]AEA or 10 µM of 2-OG containing 5 nM of [glycerol- 1,2,3-3H]2-OG as a tracer and incubated for 15 min at 37 °C under shacking. The reaction was stopped by the addition of 500 µL of ice-cold $CHCl_3$:MeOH (1:1), samples were vortexed and rapidly centrifuged at 16000 × g for 10 min at 4 °C. The aqueous phases were collected, and the radioactivity was measured for tritium content by liquid scintillation spectroscopy.

4.2.4. ABDHs assays.

ABHDs activity assays were performed as previously described [71]. Briefly, hABHD6 and hABHD12 activity was determined using cell homogenates from hABHD6 and hABHD12 stably transfected HEK293 cells. Compounds were pre-incubated with 40 µg of cell homogenate for 30 min at 37 °C in assay buffer (Tris 1 mM, EDTA 10 mM plus 0.1% BSA, pH 7.6). DMSO was used as vehicle control and WWL70 10 µM or THL 20 µM as positive controls. Then, 10 µM of 2-OG was added and incubated for 5 min at 37 °C. The reaction was stopped by the addition of 400 µL of ice-cold $CHCl_3$:MeOH (1:1). The samples were vortexed and centrifuged (16000 × g, 10 min, 4 °C). Aliquots (200 µL) of the aqueous phase were assayed for tritium content by liquid

scintillation spectroscopy. Blank values were recovered from tubes containing no enzyme. Basal 2-OG hydrolysis occurring in non-transfected HEK293 cells was subtracted.

4.3. Molecular modeling studies

Compounds **B2** was constructed with Maestro and subjected to energy minimization in a water environment (employing the Generalized-Born/surface-area model) by using Macromodel [72]. The minimization was performed until a convergence value of 0.05 kcal/(Å·mol), using the conjugated gradient method, the MMFFs as force field and a distance-dependent dielectric constant of 1.0. The ligand was docked with AUTODOCK4.2 [73] into the X-ray structure of human CB1R in complex with the agonist AM11542 (PDB code 5XRA) [74] and the recently deposited crystal structure of human CB2R in complex with antagonist AM10257 (PDB code 5ZTY) [44], which is the only human CB2R structure available at present. The docking sites were defined by setting the bound ligands as the center of a grid of 50, 60 and 50 points, respectively, in the x, y and z directions. A grid spacing of 0.375 Å and a distance-dependent function of the dielectric constant were used for the energy map calculations. The compound was subjected to 200 runs of the AUTODOCK search using the Lamarckian genetic algorithm with 10’000’000 steps of energy evaluation; as previously described [41]. The cluster analysis of the docking results was performed using an RMS tolerance of 2.0 Å. The best docking pose for each docking study was considered and the corresponding ligand-protein complex was subjected to energy minimization with AMBER 16, as previously performed for CBR-ligand complexes [75]. The complexes were embedded into a phospholipid bilayer of POPC molecules generated with VMD software [76], which was also used to place the ligand-protein complexes inside the phospholipid bilayer. The systems were solvated on both the "extracellular" and "intracellular" side with a 12 Å water cap

included in a rectangular parallelepiped water-box, using the TIP3P explicit solvent model. Chlorine ions were then added for the neutralization of the systems. Three steps of energy minimization were performed, each applying 1000 steps of steepest descent followed by 9000 steps of conjugate gradient. In the first step the phospholipids and the protein were kept fixed with a restraint of 100 kcal/(mol·Å^2), so that only the water molecules were energy minimized. During the second step the position restraint of 100 kcal/(mol·Å^2) was applied only to the receptor, thus energy minimizing the surrounding phospholipid-water environment. Finally, a third step was performed by applying a harmonic potential of 10 kcal/(mol·Å^2) only to the protein α carbons.

4.4. Pharmacological in Vitro Studies

4.4.1. Assessment of release of ILs from LPS-stimulated BV-2 Microglial Cell

Lipopolysaccharide (LPS) (Escherichia coli 0111:B4) was purchased from Sigma -Aldrich (Milan, Italy). JWH133 and SR144528 were purchased from Tocris (Ellisville, MO). Stocks of these materials in dimethyl sulfoxide (DMSO) were kept at 4 °C and diluted into cell culture medium just prior to experiments. Final DMSO concentration in culture medium didn't exceed 0.1%, a concentration, which did not show any significant effect on the investigated parameters.

The BV-2 murine microglial cells were cultured at 37 °C in a humidified atmosphere of 95% air and 5% CO_2 in high glucose Dulbecco's modified Eagle's medium (Corning, USA) supplemented with 10% heat-inactivated fetal bovine serum, streptomycin (100 g/ml), and penicillin (100 units/ml) (Sigma-Aldrich, Milan, Italy).

Microglial cells were treated with **B2** (10 μM) for 30 minutes and then stimulated with LPS (5 μg/ml). In the case of co-administration of compounds with the CB2R antagonist (SR144528, 10 μM), this latter was administered 15 minutes before agonists. After 4 hours from LPS stimulation,

the cultured media were collected and spun down for 10 minutes at 1000 × g, and the concentrations of interleukin (IL)-1β, IL-6, and IL-10 were determined by specific ELISA assays (MyBioSource, USA). All treatments and the LPS stimulation were performed in FBS-free medium, because serum showed to interfere with interleukin release (data not shown).

ELISA assay results were shown as mean ± standard error (SEM) of three independent experiments. Statistical analysis was performed by commercial software (GraphPad Prism, version 6.0 from GraphPad Software Inc., San Diego, CA, USA) using ordinary one-way ANOVA followed by Bonferroni's multiple comparison test. A p value < 0.05 was considered statistically significant.

4.4.2. Assessment of the glutamate release

4-Aminopyridine (4-AP), arachidonyl-2′-chloroethylamide hydrate (ACEA) and SR144528 were from Tocris (Bristol, UK); SR 141416A was from Selleckchem (Munich, Germany). 4-AP was dissolved in physiological medium. Stock solutions of the drugs were prepared in dimethylsulfoxide and diluted at least 1: 1000 in physiological medium; stock ACEA solution was 13.7 mM in oil and then diluted to the final concentration in physiological medium; dimethylsulfoxide diluted 1: 1000 had no effect on endogenous glutamate release.

Animals were housed at the animal care facility of the University of Genova, Department of Pharmacy (DIFAR), Italy, with constant temperature (22 ± 1 °C) and relative humidity (50%), and with 12 h light on/off cycles. Food and water were freely available. Adult rats (males, Sprague Dawley, 200–250 g) were used in accordance with the principles and procedures outlined in the EU guidelines (2010/63/EU), and with Italian Legislative Decree n. 26/2014 and were approved by the Italian Ministry of Health (protocol number 30/11/2016-OPBA of November 2016), in

accordance with Ministerial Decree 116/1992. All efforts were made to minimize the number of animals used and their suffering.

After decapitation, the hippocampus was rapidly removed and placed in ice-cold medium, and nerve terminals (purified synaptosomes) were prepared as reported previously [77,78]. In brief, the tissue was homogenized in 0.32 M sucrose, buffered at pH 7.4 with Tris-HCl. The homogenate was centrifuged at 1000g (4°C) for 5 min, and the supernatant was gently stratified on a discontinuous Percoll gradient [2, 6, 10, and 20% (v/v) in Tris-buffered sucrose] and centrifuged at 33,500g for 5 min. The layer between 10 and 20% Percoll was collected and washed by centrifugation. A standard HEPES medium was used to suspend the synaptosomes. Freshly isolated synaptosomes have been characterized in labs of the Pharmacological and Toxicological Section, DIFAR at the University of Genova, confirming negligible contamination of purified synaptosomes by astrocyte processes, microglia or oligodendrocytes [79-81].

The neurotransmitter release can be directly measured from superfused synaptosomes in superfusion. This method allows a precise pharmacological characterization of substances acting as agonists or antagonists at the characterized receptor target [82,83].

Hippocampal synaptosomes were transferred to parallel superfusion chambers at 37°C and superfused (0.5 ml/min) with standard medium. After 33-min superfusion, six superfusate fractions (B1–B6) were collected in 3-min samples; after 38 min superfusion, synaptosomes were exposed (2 min) to the depolarizing agent 4-AP (600 μM) or to CBRs agonists (ACEA 10 μM; **B2** 1 μM and 10 μM), CB1R antagonist (SR 141416A, 1 μM and 3 μM) or CB2 antagonist (SR144528 1 μM) to evaluate their effect in basal condition. To evaluate the effect of the CB1 activation on the 4-AP-evoked endogenous glutamate release the agonist ACEA (10 μM) or **B2** (1 μM and 10 μM) was added 8 min before the depolarizing stimulus and maintained in presence of 4-AP. The

effect of the CB1R antagonist SR 141416A (1 μM) or CB2R antagonist SR144528 (1 μM) was evaluated on the agonist responses by adding the compounds 8 min before 4-AP and maintained in presence of the depolarizing stimulus. In each experiment, at least two chambers were used as a control for each condition and were superfused with standard medium or with medium appropriately modified. The endogenous glutamate released in the collected sample was measured by HPLC analysis (Waters Alliance, Milford, MA, USA) as previously described [84,85]. The amount of endogenous glutamate released in the fractions was expressed as pmol/mg protein. The drug (or depolarization)-evoked glutamate efflux (overflow) was measured by subtracting the estimated basal release in appropriate control chambers from the total amount of glutamate released during stimulation in drug-treated chambers (or in chambers supplemented with 4-AP). The data are expressed as mean ± SEM of n experiments. The statistical analysis was performed using the non-parametric Mann-Whitney test to compare selected pairs of columns.

4.5. Pharmacological in vivo Studies.

4.5.1. Assessment of antinociceptive activity on oxaliplatin-induced neuropathic pain model.

Oxaliplatin-induced neuropathic pain model.

Male CD-1 albino mice (Envigo, Varese, Italy) weighing approximately 22–25 g at the beginning of the experimental procedure, were used. Animals were housed in CeSAL (Centro Stabulazione Animali da Laboratorio, University of Florence) and used at least 1 week after their arrival. Ten mice were housed per cage (size 26 × 41 cm); animals were fed a standard laboratory diet and tap water ad libitum, and kept at 23 ± 1 °C with a 12 h light/dark cycle, light at 7 a.m. All animal manipulations were carried out according to the Directive 2010/63/EU of the European parliament and of the European Union council (22 September 2010) on the protection of animals

used for scientific purposes. The ethical policy of the University of Florence complies with the Guide for the Care and Use of Laboratory Animals of the US National Institutes of Health (NIH Publication No. 85-23, revised 1996; University of Florence assurance number: A5278-01). Formal approval to conduct the experiments described was obtained from the Animal Subjects Review Board of the University of Florence. Experiments involving animals have been reported according to ARRIVE guidelines [86]. All efforts were made to minimize animal suffering and to reduce the number of animals used.

Mice treated with oxaliplatin (2.4 $mg.kg^{-1}$) were administered i.p. on days 1-2, 5-9, 12-14 (10 i.p. injections) [55,56,87]. Oxaliplatin was dissolved in 5% glucose solution. Control animals received an equivalent volume of vehicle. Behavioral tests were performed on day 15.

4.5.2. Cold plate test.

The animals were placed in a stainless steel box (12 cm × 20 cm × 10 cm) with a cold plate as floor. The temperature of the cold plate was kept constant at 4°C ± 1°C. Pain-related behavior (licking of the hind paw) was observed and the time (seconds) of the first sign was recorded. The cut-off time of the latency of paw lifting or licking was set at 60 seconds.

4.5.3. Compounds administration

B2 (5, 10, 20 and 50 $mg.kg^{-1}$) was dissolved in 1% carboxymethylcellulose and orally administered. Measurements were performed 15, 30, 45, 60 and 75 min after injection. Control mice were treated with vehicle. The selective CB1R (SR141716A; Tocris Bioscience, UK) and CB2R (SR144528; Tocris Bioscience, UK) antagonists were dissolved in saline solution with 5% DMSO and 5% Tween 20. Antagonists were administered i.p. 15 minutes before **B2** (20 $mg.kg^{-1}$ p.o.). The dosages of SR141716A and SR144528 were according to previously published articles [88,89].

4.5.4. Statistical analysis.

Behavioral measurements were performed on 16 mice for each treatment carried out in 2 different experimental sets (8 animals for single experimental session). Results were expressed as mean ± SEM. The analysis of variance of behavioral data was performed by one way ANOVA, a Bonferroni's significant difference procedure was used as post-hoc comparison. P values of less than 0.05 or 0.01 were considered significant. Investigators were blind to all experimental procedures. Data were analysed using the "Origin 9" software (OriginLab, Northampton, USA).

4.5.5. Assessment of activity on EAE model of multiple sclerosis.

Female C57BL/6J mice (7 weeks old; 15–18 g body weight) were supplied by Jackson Laboratory and kept under standard environmental conditions (24 ± 2 °C; light–dark cycle of 12:12 h) with food and water ad libitum. Mice were handled according Swiss federal legislation and protocols were approved by the respective government authorities (Veterinäramt Kanton Bern).

After one week of habituation, active EAE was induced by subcutaneous administration with 200 µg of myelin oligodendrocyte glycoprotein peptide (MOG, aa35-55) emulsified with complete Freund's adjuvant containing 4 mg/ml of Mycobacterium tuberculosis, subcutaneous injections were done in both hips and tail root. Mice were intraperitoneally administered with 300 ng of *Bordetella pertussis* toxin in PBS, after immunization and 48 h later.

Each mouse was weighted and evaluated for the presence of any clinical symptom by using a previously described scale [90]: 0, healthy; 0.5, limp tail; 1, hind legs paraparesis; 2, hind legs paraplegia; and 3, hind legs paraplegia and incontinence. Daily treatment (i.p., once a day) with

10 mg.kg^{-1} **B2** or vehicle (DMSO, 20 µL) started individually at the onset of the disease, which was observed between day 10 and 16 after immunization, and lasted for 20 days.

4.5.6. [^{35}S]GTPγS assay in mouse brains.

At the end of the EAE experiment (day 20 of treatment), mice were sacrificed, brain collected and snap frozen. As previously described, [59] frozen half brains were homogenized in a glass dounce homogenizer with 1.5 mL of ice-cold homogenization buffer (50 mM Tris-HCl, 3 mM $MgCl_2$, 1 mM EGTA, pH 7.4). Homogenates were centrifuged twice at 800 × g for 10 min at 4 °C in order to remove debris. The resulting supernatants were transferred in 2 mL plastic tubes and centrifuge at 16'000 × g for 20 min at 4 °C. The harvest membranes were re-suspended in 50 mM Tris-HCl (pH 7.4) and passed through a clean syringe, sonicated for 5 min on cold water bath, aliquoted and stored at -80 °C. Protein determination was performed using the BCA assay according to the manufacturer's instructions. For the [^{35}S]GTPγS assay, 20 µg of membrane preparation were pre-incubated in binding buffer (50 mM Tris-HCl, 3 mM $MgCl_2$, 0.2 mM EGTA, 100 mM NaCl, pH 7.4, supplemented with 0.5% BSA) for 30 min at 37 °C with 0.5 units/mL of adenosine deaminase, in the presence of 30 µM of GDP and 0.2 nM [^{35}S]GTPγS in a final volume of 200 µL. The tubes were kept on ice until binding was initiated by adding CP55,940 (1 µM), SR 141416A (1 µM), a combination of both ligands or vehicle (DMSO). Non-specific binding was measured in the presence of GTPγS (10 µM). After incubation for 1 h at 30 °C, the reaction was stopped by putting the tubes on ice. Aliquots of the reaction mixture (185 µL) were transferred to filter GF/B glass-fiber filter plates pre-soaked with ice cold 50 mM Tris-HCl plus 0.5% BSA (washing buffer). The filters were washed three times with 200 µL of washing buffer. After drying, radioactivity associated to the filters was measured in a Microbeta Trilux counter by adding 45 µL

of liquid scintillation cocktail. Results were normalized subtracting the non-specific [^{35}S]GTPγS bound to the membranes and expressed as % of vehicle control.

4.5.7. Tetrad test.

Compounds were dissolved in pure DMSO and administered i.p. at the dose of 5 mg.kg^{-1}, in a final volume of 20 μL. **B2**, **B5**, **B6** or vehicle were administered 1 h before the test. Body temperature was measured before (basal) and 1 h post injection with a thermocouple probe 1–2 cm (Physitemp Instruments Inc., Clifton, New Jersey, USA) and the change in rectal temperature was expressed as the difference between basal and post injection temperatures. Catalepsy-like behaviour was measured using the bar test, for which mice were retained in an imposed position with forelimbs resting on a bar 4 cm high, the end point of catalepsy-like behaviour was considered when both front limbs were removed (cut-off time of 120 s). Locomotion was determined using the rotarod test, for which animals were previously trained to walk over a rotarod (Erweka, Heusenstamm, Germany) at 4 rpm and for the test, the latency to fall (cut-off time of 120 s) was measured. Catalepsy-like behaviour and locomotion were measured by three trials. The hot plate test was performed to evaluate analgesia, using a 54-56 °C hot plate (Thermo Scientific, Waltham, Massachusetts, USA) with a Plexiglas cylinder, the latency to show the first nociceptive response (paw lick or foot shake) was measured.

Acknowledgment

The authors thank undergraduate Lorenzo Silicani (University of Pisa) for the contribution to the synthesis of compounds **B9** and **B10**.

Funding

This work was supported by Fism –Fondazione Italiana Sclerosi Multipla- cod 2017/R/16 and financed or co-financed with the "5 per mille" public funding.

Appendix A. Supplementary data

Supplementary data related to this article can be found at

References

[1] V. Chiurchiù, A. Leuti, M. Maccarrone. Cannabinoid signaling and neuroinflammatory diseases: A melting pot for the regulation of brain immune responses. J. Neuroimmune Pharmacol. 10 (2015) 268–280. DOI: https://doi.org/10.1007/s11481-015-9584-2.

[2] A. Stasiulewicz, K. Znajdek, M. Grudzień, T. Pawiński, A.J.I. Sulkowska. A Guide to Targeting the Endocannabinoid System in Drug Design. Int. J. Mol. Sci. 21 (2020) 2778. DOI: https://10.3390/ijms21082778.

[3] M. Tanaka, S. Sackett, Y. Zhang. Endocannabinoid Modulation of Microglial Phenotypes in Neuropathology. Front. Neurol. 11 (eCollection 2020) 87. DOI: https://10.3389/fneur.2020.00087.

[4] P. Morales, N. Jagerovic. Novel approaches and current challenges with targeting the endocannabinoid system. Expert. Opin. Drug. Discov. 27 (2020) 1-14. DOI: https://doi.org/10.1080/17460441.2020.1752178.

[5] C. Navarrete, A. García-Martin, M. Garrido-Rodríguez, L. Mestre, A. Feliú, C. Guaza, M.A. Calzado, E. Muñoz. Effects of EHP-101 on inflammation and remyelination in murine models of Multiple sclerosis Neurobiol Dis. 143 (2020) 104994. DOI: https://doi.org/10.1016/j.nbd.2020.104994

[6] A. Chicca, M.S. Gachet, V. Petrucci, W. Schuehly, R.P. Charles, J. Gertsch. 4'-O-methylhonokiol increases levels of 2-arachidonoyl glycerol in mouse brain via selective inhibition of its COX-2-mediated oxygenation. J. Neuroinflammation. 12 (2015) 89. DOI: https://doi: 10.1186/s12974-015-0307-7

[7] S. Carloni, R. Crinelli, L. Palma, F.J Álvarez, D. Piomelli, A. Duranti, W. Balduini, D. Alonso-Alconada. The Synthetic Cannabinoid URB447 Reduces Brain Injury and the Associated White Matter Demyelination after Hypoxia-Ischemia in Neonatal Rats. ACS Chem. Neurosci. 11 (2020) 1291-1299. DOI: https://doi:10.1021/acschemneuro.0c00047.

[8] J. Tomas-Roig, H.Y. Agbemenyah, N. Celarain, E. Quintana, L. Ramió-Torrentà, U. Havemann-Reinecke. Dose-dependent effect of cannabinoid WIN-55,212-2 on myelin repair following a demyelinating insult. Sci Rep. 10 (2020) 590. DOI: https://doi:10.1038/s41598-019-57290-1

[9] S.H. Choi, A.L. Arai, Y. Mou, B. Kang, C. Chern-Chyi Yen, J. Hallenbeck, A.C. Silva. Neuroprotective Effects of MAGL (Monoacylglycerol Lipase) Inhibitors in Experimental Ischemic Stroke. Stroke. 49 (2018) 718-726. DOI: https://doi:10.1161/STROKEAHA.117.019664.

[10] I. Reynoso-Moreno, A. Chicca, M.E. Flores-Soto, J.M. Viveros-Paredes, J. Gertsch. The Endocannabinoid Reuptake Inhibitor WOBE437 Is Orally Bioavailable and Exerts Indirect

Polypharmacological Effects via Different Endocannabinoid Receptors. Front. Mol. Neurosci. 11 (2018) 180. DOI: https://doi:10.3389/fnmol.2018.00180.

[11] Z.V. Varga, C. Matyas, K. Erdelyi, R. Cinar, D. Nieri, A. Chicca, B.T. Nemeth, J. Paloczi, T. Lajtos, L. Corey, G. Hasko, B. Gao, G. Kunos, J. Gertsch, P. Pacher. β-Caryophyllene protects against alcoholic steatohepatitis by attenuating inflammation and metabolic dysregulation in mice. Br J Pharmacol. 175 (2018) 320-334. DOI: https://doi:10.1111/bph.13722.

[12] V. Chiurchiù, M. Van Der Stelt, D. Centonze, M. Maccarrone. The endocannabinoid system and its therapeutic exploitation in multiple sclerosis: Clues for other neuroinflammatory diseases. Prog. Neurobiol. 160 (2018) 82–100. DOI: https://doi.org/10.1016/j.pneurobio.2017.10.007.

[13] V. Di Marzo. New approaches and challenges to targeting the endocannabinoid system. Nat. Rev. Drug Discov. 17 (2018) 623–639. DOI: https://doi.org/10.1038/nrd.2018.115.

[14] G. Pryce, D. Baker. Control of spasticity in a multiple sclerosis model is mediated by CB1, not CB2, cannabinoid receptors. Br J. Pharmacol. 150 (2007) 519-5254. DOI: https://doi.org/10.1038/sj.bjp.0707003.

[15] E. de Lago, J. Fernández-Ruiz, S. Ortega-Gutiérrez, A. Cabranes, G. Pryce, D. Baker, M. Lopez-Rodriguez, J.A. Ramos. UCM707, an inhibitor of the anandamide uptake, behaves as a symptom control agent in models of Huntington's disease and multiple sclerosis but fails to delay/arrest the progression of different motor-related disorders. Eur. Neuropsychopharmacol. 16 (2006) 7-183. DOI: https://doi.org/10.1016/j.euroneuro.2005.06.001.

[16] G. Pryce, A. Cabranes, J. Fernández-Ruiz, T. Bisogno, V. Di Marzo, J.Z. Long, B.F. Cravatt, G. Giovannoni, D. Baker. Control of experimental spasticity by targeting the

degradation of endocannabinoids using selective fatty acid amide hydrolase inhibitors. Mult. Scler. 19 (2013) 1896-1904. DOI: https://doi.org/10.1177/1352458513485982.

[17] M. Brindisi, S. Maramai, S. Gemma, S. Brogi, A. Grillo, L. Di Cesare Mannelli, E. Gabellieri, S. Lamponi, S. Saponara, B. Gorelli, D. Tedesco, T. Bonfiglio, C. Landry, K.M. Jung, A. Armirotti, L. Luongo, A. Ligresti, F. Piscitelli, C. Bertucci, M.P. Dehouck, G. Campiani, S. Maione, C. Ghelardini, A. Pittaluga, D. Piomelli, V. Di Marzo, S. Butini. Development and Pharmacological Characterization of Selective Blockers of 2-Arachidonoyl Glycerol Degradation with Efficacy in Rodent Models of Multiple Sclerosis and Pain. J. Med. Chem. 59 (2016) 2612-2632. DOI: https://doi.org/10.1021/acs.jmedchem.5b01812.

[18] J. Fernández-Ruiz, J. Romero, J.A. Ramos. Endocannabinoids and neurodegenerative disorders: Parkinson's disease, Huntington's chorea, Alzheimer's disease and others. Handb. Exp. Pharmacol. 231 (2015) 233–259. DOI: https://doi.org/10.1007/978-3-319-20825-1_8.

[19] A. Musella, H. Sepman, G. Mandolesi, A. Gentile, D. Fresegna, N. Haji, A. Conrad, B. Lutz, M. Maccarrone, D. Centonze. Pre- and postsynaptic type-1 cannabinoid receptors control the alterations of glutamate transmission in experimental autoimmune encephalomyelitis. Neuropharm. 79 (2014) 567–572. DOI: https://doi.org/10.1016/j.neuropharm.2014.01.007.

[20] A. Bernal-Chico, M. Canedo, A. Manterola, M. Victoria Sánchez-Gómez, A. Pérez-Samartín, R. Rodríguez-Puertas, C. Matute, S. Mato. Blockade of monoacylglycerol lipase inhibits oligodendrocyte excitotoxicity and prevents demyelination in vivo. Glia. 63 (2015) 163-176. DOI: https://doi.org/10.1002/glia.22742.

[21] M. Mecha, F.J. Carrillo-Salinas, A. Feliú, L. Mestre, C. Guaza. Microglia activation states and cannabinoid system: Therapeutic implications. Pharmacol. Ther. 166 (2016) 40-558. DOI: https://doi.org/10.1016/j.pharmthera.2016.06.011

[22] J. Fernández-Ruiz, C. García, O. Sagredo, M. Gómez-Ruiz, E. de Lago. The endocannabinoid system as a target for the treatment of neuronal damage. Expert. Opin. Ther. Targets. 14 (2010) 387-404. DOI: https://10.1517/14728221003709792.

[23] L. Mestre, F. Correa, A. Arévalo-Martín, E. Molina-Holgado, M. Valenti, G. Ortar, V. Di Marzo, C. Guaza. Pharmacological modulation of the endocannabinoid system in a viral model of multiple sclerosis. J. Neurochem. 92 (2005) 1327-1339. DOI: https://doi.org/10.1111/j.1471-4159.2004.02979.x.

[24] F. Gado, C. Arena, C. Fauci, I. Reynoso-Moreno, S. Bertini, M. Digiacomo, S. Meini, G. Poli, M. Macchia, T. Tuccinardi, J. Gertsch, A. Chicca, C. Manera. Modification on the 1,2-dihydro-2-oxo-pyridine-3-carboxamide Core to Obtain Multi-Target Modulators of Endocannabinoid System. Bioorg Chem 94 (2020) 103353. DOI: https://doi.org/10.1016/j.bioorg.2019.103353

[25] A. Chicca, C. Arena, S. Bertini, F. Gado, E. Ciaglia, M. Abate, M. Digiacomo, M. Lapillo, G. Poli, M. Bifulco, M. Macchia, T. Tuccinardi, J. Gertsch, C..Manera, Polypharmacological profile of 1,2-dihydro-2-oxo-pyridine-3-carboxamides in the endocannabinoid system. Eur. J. Med. Chem. 154 (2018) 155-171. DOI: https://doi:10.1016/j.ejmech.2018.05.019.

[26] Chicca, D. Caprioglio, A. Minassi, V. Petrucci, G. Appendino, O. Taglialatela-Scafati, J. Gertsch. Functionalization of β-caryophyllene generates novel polypharmacology in the endocannabinoid system. ACS Chem. Biol. 9 (2014) 1499–1507. DOI: https://doi.org/10.1021/cb500177c.

[27] T.R. Pardo-García, N. Yusif-Rodriguez, G. Yudowski, C.S. Maldonado-Vlaar. Blockade of the endovanilloid receptor, TRPV1, and of the endocannabinoid enzyme, FAAH, within the

nucleus accumbens shell elicits anxiolytic-like effects in male rats. Neurosci. Lett. 732 (2020) 135023. DOI: https://doi:10.1016/j.neulet.2020.135023

[28] M.C. Goodman, S. Xu, C.A. Rouzer, S. Banerjee, K. Ghebreselasie, M. Migliore, D. Piomelli, L.J. Marnett. Dual cyclooxygenase-fatty acid amide hydrolase inhibitor exploits novel binding interactions in the cyclooxygenase active site. J. Biol. Chem. 293 (2018) 3028-3038. DOI: https://doi:10.1074/jbc.M117.802058.

[29] M. Bashashati, J. Fichna, F. Piscitelli, R. Capasso, A.A. Izzo, A. Sibaev, J.P. Timmermans, N. Cenac, N. Vergnolle, V. Di Marzo, M. Storr. Targeting fatty acid amide hydrolase and transient receptor potential vanilloid-1 simultaneously to modulate colonic motility and visceral sensation in the mouse: A pharmacological intervention with N-arachidonoyl-serotonin (AA-5-HT). Neurogastroenterol. Motil. 29 (2017) 10.1111/nmo.13148. DOI: https://doi:10.1111/nmo.13148.

[30] N. Malek, M. Mrugala, W. Makuch, N. Kolosowska, B. Przewlocka, M. Binkowski, M. Czaja, E. Morera, V. Di Marzo, K. Starowicz. A multi-target approach for pain treatment: dual inhibition of fatty acid amide hydrolase and TRPV1 in a rat model of osteoarthritis. Pain. 156 (2015) 890-903. DOI: https://doi:10.1097/j.pain.0000000000000132.

[31] A. Navarria, A. Tamburella, F.A. Iannotti, V. Micale, G. Camillieri, L. Gozzo, R. Verde, R. Imperatore, G.M. Leggio, F. Drago, V. Di Marzo. The dual blocker of FAAH/TRPV1 N-arachidonoylserotonin reverses the behavioral despair induced by stress in rats and modulates the HPA-axis. Pharmacol. Res. 87 (2014) 151-159. DOI: https://doi:10.1016/j.phrs.2014.04.014.

[32] V. Lucchesi, T. Parkkari, J.R. Savinainen, A.M. Malfitano, M. Allarà, S. Bertini, F. Castelli, S. Del Carlo, C. Laezza, A. Ligresti, G. Saccomanni, M. Bifulco, V. Di Marzo, M.

Macchia, C. Manera. 1,2-Dihydro-2-oxopyridine-3-carboxamides: the C-5 substituent is responsible for functionality switch at CB2 cannabinoid receptor Eur. J. Med. Chem. 74 (2014) 524-532. DOI: https://doi: 10.1016/j.ejmech.2013.10.070.

[33] Manera C, Saccomanni G, Malfitano AM, Bertini S, Castelli F, Laezza C, Ligresti A, Lucchesi V, Tuccinardi T, Rizzolio F, Bifulco M, Di Marzo V, Giordano A, Macchia M, Martinelli A. Rational design, synthesis and anti-proliferative properties of new CB2 selective cannabinoid receptor ligands: an investigation of the 1,8-naphthyridin-2(1H)-one scaffold. Eur. J. Med. Chem. 52 (2012) 284-294. DOI: https://doi: 10.1016/j.ejmech.2012.03.031.

[34] F. Micoli, P. Costantino, R. Adamo. Potential targets for next generation antimicrobial glycoconjugate vaccines. FEMS Microbiol. Rev. 42 (2018) 388-423. DOI: https://doi.org/10.1093/femsre/fuy011.

[35] L. Guazzelli, O. McCabe, S. Oscarson. Synthesis of part structures of Cryptococcus neoformans serotype C capsular polysaccharide. Carbohydr. Res. 433 (2016) 5-13. DOI: https://doi.org/10.1016/j.carres.2016.06.012.

[36] L. Guazzelli, G. Catelani, F. D'Andrea. Lactose as an inexpensive starting material for the preparation of aldohexos-5-uloses: synthesis of L-ribo and D-lyxo derivatives. Carbohydr. Res. 345 (2010) 369-376. DOI: https://doi.org/10.1016/j.carres.2009.11.027.

[37] R. Bianchini, M. Rolla, J. Isaad, G. Catelani, L. Guazzelli, M. Corsi, M.R. Bonanni. Efficient Double Glycoconjugation to Naturalize High Molecular Weight Disperse Dyes. Carbohydr. Res. 356 (2012) 104-109. DOI: https://doi.org/10.1016/j.carres.2011.10.036.

[38] M. Landi, G. Catelani, F. D'Andrea, E. Ghidini, G. Amari, P. Puccini, N. Bianchi, R. Gambari. Synthesis of glycose carbamides and evaluation of the induction of erythroid

differentiation of human erythroleukemic K562 cells. Eur. J. Med. Chem. 44 (2009) 745-754. DOI: https://doi.org/10.1016/j.ejmech.2008.05.001.

[39] E. Nuti, D. Cuffaro, F. D'Andrea, L. Rosalia, L. Tepshi, M. Fabbi, G. Carbotti, S. Ferrini, S. Santamaria, C. Camodeca, L. Ciccone, E. Orlandini, S. Nencetti, E.A. Stura, V. Dive, A. Rossello. Sugar-Based Arylsulfonamide Carboxylates as selective and water-soluble matrix metalloproteinase-12 inhibitors. ChemMedChem 11 (2016) 1626–1637. DOI: https://doi.org/10.1002/cmdc.201600235.

[40] A. Daina, O. Michielin, V. Zoete. SwissADME: a free web tool to evaluate pharmacokinetics, drug-likeness and medicinal chemistry friendliness of small molecules. Sci. Rep. 7 (2017) 42717. DOI: https://doi.org/10.1038/srep42717.

[41] G. Bononi, C. Granchi, M. Lapillo, M. Giannotti, D. Nieri, S. Fortunato, M.E. Boustani, I. Caligiuri, G. Poli, K.E. Carlson, S.H. Kim, M. Macchia, A. Martinelli, F. Rizzolio, A. Chicca, J.A. Katzenellenbogen, F. Minutolo, T. Tuccinardi. Discovery of long-chain salicylketoxime derivatives as monoacylglycerol lipase (MAGL) inhibitors. Eur. J. Med. Chem. 157 (2018) 817-836. DOI: https://doi.org/10.1016/j.ejmech.2018.08.038.

[42] M. Lapillo, T. Tuccinardi, A. Martinelli, M. Macchia, A. Giordano, G. Poli. Extensive Reliability Evaluation of Docking-Based Target-Fishing Strategies. Int. J. Mol. Sci. 20 (2019) 1023. DOI: https://doi.org/10.3390/ijms20051023.

[43] T. Hua, K. Vemuri, M. Pu, L. Qu, G.W. Han, Y. Wu, S. Zhao, W. Shui, S. Li, A. Korde, R.B. Laprairie, E.L. Stahl, J.H. Ho, N. Zvonok, H. Zhou, I. Kufareva, B. Wu, Q. Zhao, M.A. Hanson, L.M. Bohn, A. Makriyannis, R.C. Stevens, Z.J. Liu. Crystal Structure of the Human Cannabinoid Receptor CB1. Cell. 167 (2016) 750-762. DOI: https://doi.org/10.1016/j.cell.2016.10.004.

[44] X. Li, T. Hua, K. Vemuri, J.H. Ho, Y. Wu, L. Wu, P. Popov, O. Benchama, N. Zvonok, K. Locke,L. Qu, G.W. Han, M.R. Iyer, R. Cinar, N.J. Coffey, J. Wang, M. Wu, V. Katritch, S. Zhao, G. Kunos, L.M. Bohn, A. Makriyannis, R.C. Stevens, Z.J. Liu. Crystal Structure of the Human Cannabinoid Receptor CB2. Cell. 176 (2019) 459-467. DOI: https://doi.org/10.1016/j.cell.2018.12.011.

[45] E. Kozela, M. Pietr, A. Juknat, N. Rimmerman, R. Levy, Z. Vogel. Cannabinoids Δ 9 -Tetrahydrocannabinol and Cannabidiol Differentially Inhibit the Lipopolysaccharide-activated NF-κB and Interferon-β/STAT Proinflammatory Pathways in BV-2 Microglial Cells. J. Biol. Chem. 285 (2010) 1616–1626. DOI: 10.1074/jbc.M109.069294.

[46] E. Janefjord, J.L.V. Mååg, B.S. Harvey, S.D. Smid. Cannabinoid Effects on β Amyloid Fibril and Aggregate Formation, Neuronal and Microglial-Activated Neurotoxicity In Vitro. Cell. Mol. Neurobiol. 34 (2014) 31–42. DOI: https://doi.org/10.1007/s10571-013-9984-x.

[47] N. Malek, K. Popiolek-Barczyk, J. Mika, B. Przewlocka, K. Starowicz. Anandamide, Acting via CB2 Receptors, Alleviates LPS-Induced Neuroinflammation in Rat Primary Microglial Cultures. Neural Plasticity. 2015 (2015) 1–10. DOI: https://doi.org/10.1155/2015/130639.

[48] A.M. Martín-Moreno, D. Reigada, B.G. Ramirez, R. Mechoulam, N.G. Innamorato, A. Cuadrado, M.L. de Ceballos. Cannabidiol and other cannabinoids reduce microglial activation in vitro and in vivo: relevance to Alzheimer's disease. Mol. Pharmacol. 79 (2011) 964–973. DOI: https://doi.org/10.1124/mol.111.071290

[49] L. Walter, A. Franklin, A. Witting, C. Wade, Y. Xie, G. Kunos, K. Mackie, N. Stella. Nonpsychotropic Cannabinoid Receptors Regulate Microglial Cell Migration. J. Neurosci. 23 (2003) 1398–1405. DOI: https://doi.org/10.1523/JNEUROSCI.23-04-01398.2003.

[50] L. Ma, J. Jia, X. Liu, F. Bai, Q. Wang, L. Xiong. Activation of murine microglial N9 cells is attenuated through cannabinoid receptor CB2 signaling. Biochem. Biophys. Res. Comm. 458 (2015) 92–97. DOI: https://doi.org/10.1016/j.bbrc.2015.01.073.

[51] E. Polazzi, B. Monti. Microglia and neuroprotection: From in vitro studies to therapeutic applications. Progr. Neurobiol. 92 (2010) 293–315. DOI: https://doi.org/10.1016/j.pneurobio.2010.06.009.

[52] C. Cannizzaro, M. D'Amico, P. Preziosi, M. Martire. Presynaptic effects of anandamide and WIN55,212-2 on glutamatergic nerve endings isolated from rat hippocampus. Neurochem Int. 48 (2006) 159-165. DOI: https://doi.org/10.1016/j.neuint.2005.10.009.

[53] R.M. Bitencourt, A. Alpár, V. Cinquina, S.G. Ferreira, B.S. Pinheiro, C. Lemos, C. Ledent, R.N. Takahashi, F.J. Sialana, G. Lubec, R.A. Cunha, T. Harkany, A. Köfalvi. Lack of presynaptic interaction between glucocorticoid and CB1 cannabinoid receptors in GABA- and glutamatergic terminals in the frontal cortex of laboratory rodents. Neurochem Int. 90 (2015) 72-84. DOI: https://doi.org/10.1016/j.neuint.2015.07.014.

[54] M. D'Amico, C. Cannizzaro, P. Preziosi, M. Martire. Inhibition by anandamide and synthetic cannabimimetics of the release of [3H]D-aspartate and [3H]GABA from synaptosomes isolated from the rat hippocampus. Neurochem Res. 29 (2004) 1553-1561. DOI: https://doi.org/10.1023/B:NERE.0000029569.20266.3f.

[55] L. Di Cesare Mannelli, E. Lucarini, L. Micheli, I. Mosca, P. Ambrosino, M.V. Soldovieri, A. Martelli, L. Testai, M. Taglialatela, V. Calderone, C. Ghelardini. Effects of natural and synthetic isothiocyanate-based H2S-releasers against chemotherapy-induced neuropathic pain: role of Kv7 potassium channels. Neuropharmacology. 121 (2017) 49−59. DOI: https://doi.org/10.1016/j.neuropharm.2017.04.029.

[56] F. Gado, L. Di Cesare Mannelli, E. Lucarini, S. Bertini, E. Cappelli, M. Digiacomo, L.A. Stevenson, M. Macchia, T. Tuccinardi, C. Ghelardini, R.G. Pertwee, C. Manera. Identification of the First Synthetic Allosteric Modulator of the CB2 Receptors and Evidence of Its Efficacy for Neuropathic Pain Relief. J. Med. Chem. 62 (2019) 276-287. DOI: https://doi.org/10.1021/acs.jmedchem.8b00368.

[57] M. Metna-Laurent, M. Mondésir, A. Grel, M. Vallée, P.V. Piazza. Cannabinoid-Induced Tetrad in Mice. Curr. Protoc. Neurosci. 80 (2017) 9.59.1-9.59.10. DOI: https://doi.org/10.1002/cpns.31.

[58] A. Chicca, M.A. Schafroth, I. Reynoso-Moreno, R. Erni, V. Petrucci, E.M. Carreira, J. Gertsch. Uncovering the psychoactivity of a cannabinoid from liverworts associated with a legal high. Sci. Adv. 4 (2018) eaat2166. DOI: https://10.1126/sciadv.aat2166.

[59] A. Chicca, S. Nicolussi, R. Bartholomäus, M. Blunder, A. Aparisi Rey, V. Petrucci, I. Reynoso-Moreno, J.M. Viveros-Paredes, M. Dalghi Gens, B. Lutz, H.B. Schiöth, M. Soeberdt, C. Abels, R.P. Charles, K.H. Altmann, J. Gertsch. Chemical probes to potently and selectively inhibit endocannabinoid cellular reuptake. Proc. Natl. Acad. Sci. U S A. 114 (2017) E5006-E5015. DOI: https://doi.org/10.1073/pnas.1704065114.

[60] F. Docagne, L. Mestre, F. Loría, M. Hernangómez, F. Correa, C. Guaza. Therapeutic potential of CB2 targeting in multiple sclerosis. Expert Opin. Ther. Targets. 12 (2008) 185–195. DOI: 10.1517/14728222.12.2.185.

[61] C. Turcotte, M.-R. Blanchet, M. Laviolette, N. Flamand. The CB2 receptor and its role as a regulator of inflammation. Cell Mol. Life Sci. 73 (2016) 4449–4470. DOI: https://doi.org/10.1007/s00018-016-2300-4.

[62] B.G. Ramírez, C. Blázquez, T. Gómez del Pulgar, M. Guzmán, M.L. de Ceballos. Prevention of Alzheimer's disease pathology by cannabinoids: neuroprotection mediated by blockade of microglial activation. J. Neurosci. 25 (2005) 1904–1913. DOI: https://doi.org/10.1523/JNEUROSCI.4540-04.2005.

[63] L. Jean-Gilles, M. Braitch, M.L. Latif, J. Aram, A.J. Fahey, L.J. Edwards, R.A. Robins, R. Tanasescu, P.J. Tighe, B. Gran, L.C. Showe, S. P. Alexander, V. Chapman, D. A. Kendall, C.S. Constantinescu. Effects of pro-inflammatory cytokines on cannabinoid CB1 and CB2 receptors in immune cells. Acta Physiol (Oxf) 214 (2015) 63–74. DOI: https://doi.org/10.1111/apha.12474

[64] M. Roche, J.P. Kelly, M. O'Driscoll, D.P. Finn. Augmentation of endogenous cannabinoid tone modulates lipopolysaccharide-induced alterations in circulating cytokine levels in rats. Immunology. 125 (2008) 263–271. DOI: https://doi.org/10.1111/j.1365-2567.2008.02838.x.

[65] A. Rubio-Araiz, A. Arévalo-Martín, O. Gómez-Torres, B. Navarro-Galve, D. García-Ovejero, P. Suetterlin, E. Sánchez-Heras, E. Molina-Holgado, F. Molina-Holgado. The endocannabinoid system modulates a transient TNF pathway that induces neural stem cell proliferation. Mol. Cell. Neurosci. 38 (2008) 374–380. DOI: https://doi.org/10.1016/j.mcn.2008.03.010.

[66] K.M. King, A.M. Myers, A.J. Soroka-Monzo, R.F. Tuma, R.J. Tallarida, E.A. Walker, S.J. Ward. Single and combined effects of Δ9 -tetrahydrocannabinol and cannabidiol in a mouse model of chemotherapy-induced neuropathic pain. Br. J. Pharmacol. 174 (2017) 2832-2841. DOI: https://10.1111/bph.13887.

[67] D. Pascual, C. Goicoechea, M. Suardiaz, M.I. Martin A cannabinoid agonist, WIN 55,212-2, reduces neuropathic nociception induced by paclitaxel in rats. Pain 118 (2005) 23–34. DOI: https://10.1016/j.pain.2005.07.008.

[68] E.J. Rahn, A. Makriyannis, A.G. Hohmann. Activation of cannabinoid CB1 and CB2 receptors suppresses neuropathic nociception evoked by the chemotherapeutic agent vincristine in rats. Br. J. Pharmacol. 152 (2007) 765–777. DOI: https://10.1038/sj.bjp.0707333.

[69] D.D. Perrin, W.L.F. Armarego, D.R. Perrin. Purification of Laboratory Chemicals, 2nd ed., Pergamon Press, Oxford, 1980.

[70] C. Granchi, M. Lapillo, S. Glasmacher, G. Bononi, C. Licari, G. Poli, M. El Boustani, I. Caligiuri, F. Rizzolio, J. Gertsch, M. Macchia, F. Minutolo, T. Tuccinardi, A. Chicca. Optimization of a Benzoylpiperidine Class Identifies a Highly Potent and Selective Reversible Monoacylglycerol Lipase (MAGL) Inhibitor. J. Med. Chem. 62 (2019) 1932-1958. DOI: https://doi.org/10.1021/acs.jmedchem.8b01483.

[71] V. Petrucci, A. Chicca, S. Glasmacher, J. Paloczi, Z. Cao, P. Pacher, J. Gertsch. Pepcan-12 (RVD-hemopressin) is a CB2 receptor positive allosteric modulator constitutively secreted by adrenals and in liver upon tissue damage. Sci. Rep. 7 (2017) 9560. DOI: https://doi.org/10.1038/s41598-017-09808-8.

[72] Macromodel, Version 9.7, Schr€odinger, Inc., New York, 2009.

[73] G.M. Morris, R. Huey, W. Lindstrom, M.F. Sanner, R.K. Belew, D.S. Goodsell, A.J. Olson. AutoDock4 and AutoDockTools4: automated docking with selective receptor flexibility. J. Comput. Chem. 30 (2009) 2785–2791. DOI: https://doi.org/10.1002/jcc.21256.

[74] T. Hua, K. Vemuri, S.P. Nikas, R.B. Laprairie, Y. Wu, L. Qu, M. Pu, A. Korde, S. Jiang, J.H. Ho, G.W. Han, K. Ding, X. Li, H. Liu, M.A. Hanson, S. Zhao, L.M. Bohn, A.

Makriyannis, R.C. Stevens, Z.J. Liu. Crystal structures of agonist-bound human cannabinoid receptor CB1. Nature. 547 (2017) 468-471. DOI: https://doi.org/10.1038/nature23272.

[75] M. Aghazadeh Tabrizi, P.G. Baraldi, E. Ruggiero, G. Saponaro, S. Baraldi, G. Poli, T. Tuccinardi, A. Ravani, F. Vincenzi, P.A. Borea, K. Varani. Synthesis and structure activity relationship investigation of triazolo[1,5-a]pyrimidines as CB2 cannabinoid receptor inverse agonists. Eur. J. Med. Chem. 113 (2016) 11-27. DOI: https://doi.org/10.1016/j.ejmech.2016.02.032.

[76] W. Humphrey, A. Dalke, K. Schulten. VMD: visual molecular dynamics, J. Mol.Graph. 14 (1996) 33-38.

[77] M. Pedrazzi, M. Averna, B. Sparatore, M. Patrone, F. Salamino, M. Marcoli, G. Maura, C. Cervetto, D. Frattaroli, S. Pontremoli, E. Melloni. Potentiation of NMDA receptor-dependent cell responses by extracellular high mobility group box 1 protein. PLoS One. 7 (2012) e44518. DOI: 10.1371/journal.pone.0044518.

[78] M. Averna, M. Pellegrini, C. Cervetto, M. Pedrazzi, M. Bavestrello, R. De Tullio, F. Salamino, S. Pontremoli, E. Melloni. Physiological roles of calpain 1 associated to multiprotein NMDA receptor complex. PloS one. 10 (2015) e0139750. DOI: 10.1371/journal.pone.0139750.

[79] C. Cervetto, L. Vergani, M. Passalacqua, M. Ragazzoni, A. Venturini, F. Cecconi, N. Berretta, N. Mercuri, M. D'Amelio, G. Maura, P. Mariottini, A. Voci, M. Marcoli, M. Cervelli. Astrocyte-dependent vulnerability to excitotoxicity in spermine oxidase-overexpressing mouse. Neuromol. Med. 18 (2016) 50-68. DOI: https://doi.org/10.1007/s12017-015-8377-3.

[80] C. Cervetto, A. Venturini, M. Passalacqua, D. Guidolin, S. Genedani, K. Fuxe, D.O. Borroto-Esquela, P. Cortelli, A. Woods, G. Maura, M. Marcoli, L.F. Agnati. A2A-D2

receptor–receptor interaction modulates gliotransmitter release from striatal astrocyte processes. J. Neurochem. 140 (2017) 268-279. DOI: https://doi.org/10.1111/jnc.13885.

[81] A. Venturini, M. Passalacqua, S. Pelassa, F. Pastorino, M. Tedesco, K. Cortese, M.C. Gagliani, G. Leo, G. Maura, D. Guidolin, L.F. Agnati, M. Marcoli, C. Cervetto. Exosomes from astrocyte processes: signaling to neurons. Front. Pharmacol. 10 (2019) 1452. DOI: https://doi.org/10.3389/fphar.2019.01452.

[82] C. Cervetto, D. Frattaroli, A. Venturini, M. Passalacqua, M. Nobile, S. Alloisio, C. Tacchetti, G. Maura, L.F. Agnati, M. Marcoli. Calcium-permeable AMPA receptors trigger vesicular glutamate release from Bergmann gliosomes. Neuropharmacol. 99 (2015) 396-407. DOI: https://doi.org/10.1016/j.neuropharm.2015.08.011.

[83] L. Di Cesare Mannelli, M. Marcoli, L. Micheli, M. Zanardelli, G. Maura, C. Ghelardini, C. Cervetto. Oxaliplatin evokes P2X7-dependent glutamate release in the cerebral cortex: A pain mechanism mediated by Pannexin 1. Neuropharmacol. 97 (2015) 133-141. DOI: https://doi.org/10.1016/j.neuropharm.2015.05.037.

[84] M. Marcoli, C. Cervetto, M. Castagnetta, P. Sbaffi, G. Maura. 5-HT control of ischemia-evoked glutamate efflux from human cerebrocortical slices. Neurochem. Intern. 45 (2004) 687-691. DOI: https://doi.org/10.1016/j.neuint.2004.03.004.

[85] A. Amaroli, M. Marcoli, A. Venturini, M. Passalacqua, L.F. Agnati, A. Signore, M. Raffetto, G. Maura, S. Benedicenti, C. Cervetto. Near-infrared laser photons induce glutamate release from cerebrocortical nerve terminals. J. Biophotonics. 11 (2018) e201800102. DOI: https://doi.org/10.1002/jbio.201800102.

[86] J.C. McGrath, E. Lilley. Implementing guidelines on reporting research using animals (ARRIVE etc.): new requirements for publication in BJP. Br. J. Pharmacol. 172 (2015) 3189−3193. DOI: https://doi.org/10.1111/bph.12955.

[87] G. Cavaletti, G. Tredici, M.G. Petruccioli, E. Donde, P. Tredici, P. Marmiroli, C. Minoia, A. Ronchi, M. Bayssas, G.G. Etienne. Effects of different schedules of oxaliplatin treatment on the peripheral nervous system of the rat. Eur. J. Cancer. 37 (2001) 2457−2463. DOI: https://doi.org/10.1016/S0959-8049(01)00300-8.

[88] K.D. Lake, D.R. Compton, K. Varga, B.R. Martin, G. Kunos. Cannabinoid-induced hypotension and bradycardia in rats mediated by CB1-like cannabinoid receptors. J. Pharmacol. Exp. Ther. 281 (1997) 1030−1037.

[89] A.L. Li, L.M. Carey, K.M. Mackie, A.G. Hohmann. Cannabinoid CB2 Agonist GW405833 Suppresses Inflammatory and Neuropathic Pain through a CB1 Mechanism that is Independent of CB2 Receptors in Mice. J. Pharmacol. Exp. Ther. 362 (2017) 296−305. DOI: https://doi.org/10.1124/jpet.117.241901.

[90] S.M. Tietz, M. Zwahlen, N. Haghayegh Jahromi, P. Baden, I. Lazarevic, G. Enzmann, B. Engelhardt. Refined clinical scoring in comparative EAE studies does not enhance the chance to observe statistically significant differences. Eur J Immunol. 46 (2016) 2481-2483. DOI: https://doi.org/10.1002/eji.201546272.